

ISSN: (Print) (Online) Journal homepage: <https://www.tandfonline.com/loi/tbsd20>

Exploring natural products as multi-target-directed drugs for Parkinson's disease: an *in-silico* approach integrating QSAR, pharmacophore modeling, and molecular dynamics simulations

Yassir Boulaamane, Iman Touati, Nainee Goyal, Anshuman Chandra, Lokesh Kori, Mahmoud A. A. Ibrahim, Mohammed Reda Britel & Amal Maurady

To cite this article: Yassir Boulaamane, Iman Touati, Nainee Goyal, Anshuman Chandra, Lokesh Kori, Mahmoud A. A. Ibrahim, Mohammed Reda Britel & Amal Maurady (27 Sep 2023): Exploring natural products as multi-target-directed drugs for Parkinson's disease: an *in-silico* approach integrating QSAR, pharmacophore modeling, and molecular dynamics simulations, Journal of Biomolecular Structure and Dynamics, DOI: [10.1080/07391102.2023.2260879](https://doi.org/10.1080/07391102.2023.2260879)

To link to this article: <https://doi.org/10.1080/07391102.2023.2260879>



View supplementary material [↗](#)



Published online: 27 Sep 2023.



Submit your article to this journal [↗](#)



View related articles [↗](#)



View Crossmark data [↗](#)



Exploring natural products as multi-target-directed drugs for Parkinson's disease: an *in-silico* approach integrating QSAR, pharmacophore modeling, and molecular dynamics simulations

Yassir Boulaamane^a, Iman Touati^a, Nainee Goyal^b, Anshuman Chandra^c, Lokesh Kori^c, Mahmoud A. A. Ibrahim^{d,e}, Mohammed Reda Britel^a and Amal Maurady^{a,f}

^aLaboratory of Innovative Technologies, National School of Applied Sciences of Tangier, Abdelmalek Essaadi University, Tetouan, Morocco;

^bSchool of Biotechnology, Gautam Buddha University, Greater Noida, India; ^cICMR-National Institute of Malaria Research, Dwarka, New Delhi, India; ^dChemistry Department, Faculty of Science, Computational Chemistry Laboratory, Minia University, Minia, Egypt; ^eSchool of Health Sciences, University of KwaZulu-Natal, Westville, Durban, South Africa; ^fFaculty of Sciences and Techniques of Tangier, Abdelmalek Essaadi University, Tetouan, Morocco

Communicated by Ramaswamy H. Sarma.

ABSTRACT

Parkinson's disease is a neurodegenerative disorder characterized by the progressive loss of dopaminergic neurons in the midbrain. Current treatments provide limited symptomatic relief without halting disease progression. A multi-targeting approach has shown potential benefits in treating neurodegenerative diseases. In this study, we employed *in silico* approaches to explore the COCONUT natural products database and identify novel drug candidates with multi-target potential against relevant Parkinson's disease targets. QSAR models were developed to screen for potential bioactive molecules, followed by a hybrid virtual screening approach involving pharmacophore modeling and molecular docking against MAO-B, AA_{2A}R, and NMDAR. ADME evaluation was performed to assess drug-like properties. Our findings revealed 22 candidates that exhibited the desired pharmacophoric features. Particularly, two compounds: CNP0121426 and CNP0242698 exhibited remarkable binding affinities, with energies lower than -10 kcal/mol and promising interaction profiles with the chosen targets. Furthermore, all the ligands displayed desirable pharmacokinetic properties for brain-targeted drugs. Lastly, molecular dynamics simulations were conducted on the lead candidates, belonging to the dihydrochalcone and curcuminoid class, to evaluate their stability over a 100 ns timeframe and compare their dynamics with reference complexes. Our findings revealed the curcuminoid CNP0242698 to have an overall better stability with the three targets compared to the dihydrochalcone, despite the high ligand RMSD, the curcuminoid CNP0242698 showed better protein stability, implying ligand exploration of different orientations. Similarly, AA_{2A}R exhibited higher stability with CNP0242698 compared to the reference complex, despite the high initial ligand RMSD due to the bulkier active site. In NMDAR, CNP0242698 displayed good stability and less fluctuations implying a more restricted conformation within the smaller active site of NMDAR. These results may serve as lead compounds for the development and optimization of natural products as multi-target disease-modifying natural remedies for Parkinson's disease patients. However, experimental assays remain necessary to validate these findings.

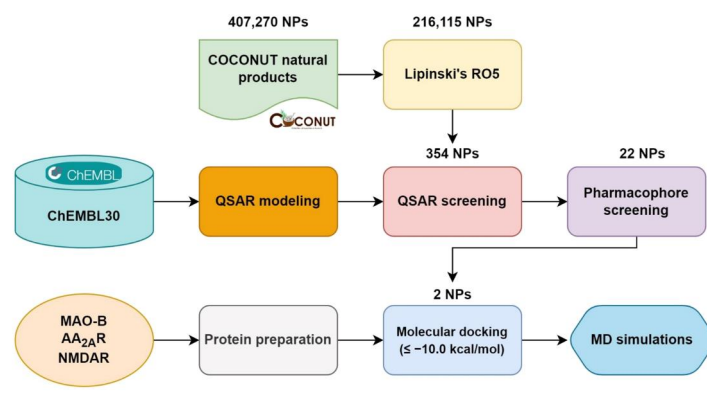
ARTICLE HISTORY




Received 26 April 2023


Accepted 14 September 2023

KEYWORDS

ADME prediction; molecular dynamics simulations; multi-target-directed ligands; natural products; Parkinson's disease; QSAR modeling



CONTACT Anshuman Chandra  anshuman@nimr.org.in  ICMR-National Institute of Malaria Research, Dwarka, New Delhi, India; Amal Maurady  amal.maurady.ma@gmail.com; amaurady@uae.ac.ma  Laboratory of Innovative Technologies, National School of Applied Sciences of Tangier, Abdelmalek Essaadi University, Tetouan, Morocco

 Supplemental data for this article can be accessed online at <https://doi.org/10.1080/07391102.2023.2260879>.

© 2023 Informa UK Limited, trading as Taylor & Francis Group

1. Introduction

Neurodegenerative disorders are incurable conditions that result in the progressive degeneration of nerve cells in the brain (Barnham et al., 2004). Neurodegenerative diseases such as Alzheimer's, Huntington's, and Parkinson's diseases have complex and multifactorial natures because of the different factors contributing to their progression (Ibrahim & Gabr, 2019). Neurodegenerative diseases lead to increased mortality and morbidity in older patients and are a great burden on society, where there is currently no approved treatment to prevent the progression of these diseases (Van der Schyf, 2011). Parkinson's disease (PD) is considered the second most frequent neurological disorder that is described by the loss of dopaminergic neurons in the midbrain (Dauer & Przedborski, 2003). Current therapeutic approaches for the treatment of PD offer limited symptomatic benefits to patients with no prevention of neuronal loss (Rascol et al., 2003). Accumulating evidence indicates that oxidative damage and mitochondrial imbalance contribute to the cascade of events leading to the degeneration of these dopaminergic neurons (Jenner, 2003). Given the susceptibility of resistance concerning drugs that act on one therapeutic target and the multifactorial nature of neurodegenerative diseases, it has become necessary to develop new treatment strategies. In this regard, scientists have become convinced that the polypharmacological approach targeting multiple proteins linked to the development and progression of the disease should prove to be more beneficial to patients than the current approaches (Lang, 2010; Piau et al., 2011).

Monoamine Oxidase (MAO) is a mitochondrial flavoenzyme that catalyzes the metabolism of some neurotransmitters such as dopamine (Youdim et al., 2006). It is expressed in two isoforms—namely MAO-A and MAO-B that share about 70% of their sequence identity but differ by their tissue distribution, substrates, and inhibitors preferences (Wang et al., 2013). MAO-A preferentially degrades serotonin while MAO-B preferentially metabolizes 2-phenylethylamine and benzylamine. Dopamine, adrenaline, and noradrenaline are substrates of both isoenzymes (Finberg & Rabey, 2016).

The use of MAO-A inhibitors has been abandoned since the discovery that their use can cause a hypertensive crisis which is related to the metabolism of tyramine (Yamada & Yasuhara, 2004). However, a new generation of selective MAO-B inhibitors proved to be relevant especially when considering that the brain shows an age-related increase in MAO-B activity in patients with PD (Carradori & Silvestri, 2015). During aging, the expression of MAO-B increases in the brain and relates to an enhanced dopamine metabolism which results in an increased reactive oxygen species (ROS) production such as hydrogen peroxide (H_2O_2) inducing oxidative damage and apoptotic signaling events (Lotharius & Brundin, 2002). Given these concerns, MAO-B inhibitors could offer both symptomatic and neuroprotective activities (Tabakman et al., 2004).

Adenosine A_{2A} receptor ($AA_{2A}R$) is another successful drug target for PD, it represents one of the three subtypes of the adenosine receptor, a G protein-coupled receptor formed by seven transmembrane α -helices (de Lera Ruiz et al., 2014).

The link between $AA_{2A}R$ and PD stems from the link that $AA_{2A}R$ activation counteracts the actions of dopamine, a key neurotransmitter to motor control. Therefore, the blockade of $AA_{2A}R$ through the administration of its antagonists could help with PD motor symptoms. Moreover, oral administration of $AA_{2A}R$ antagonists in experimental models prevented the loss of dopaminergic neurons suggesting their neuroprotective properties (Ikeda et al., 2002).

N-methyl-D-aspartate receptor (NMDAR) is also considered a relevant target for treating PD through receptor-mediated neuroprotection (Hardingham, 2009). NMDAR is a glutamate receptor and ion channel found in neurons, it represents one of three types of ionotropic glutamate receptors, with the other two being AMPA (α -amino-3-hydroxy-5-methyl-4-isoxazolepropionic acid) and kainate receptors (Gonda, 2012). It was demonstrated that the excitatory neurotransmitter, glutamate, contributes to the processes of PD (Iovino et al., 2020). Moreover, it was found that PD patients have higher serum concentrations of glutamate when compared to healthy subjects (Mironova et al., 2018). Whereas NMDAR antagonists display beneficial effects on reversing motor symptoms, reducing levodopa-induced dyskinesia, and slowing progressive neurodegeneration in preclinical PD models (Stoof et al., 1992). Therefore, NMDAR represents a promising target as a therapeutic non-dopaminergic intervention by reversing the severe motor complications that derive from the current dopamine replacement strategies (Zhang et al., 2019).

Recently, there has been a shift of interest in plants and natural products (NPs) when seeking novel remedies for various diseases. NPs and their derivatives have been recognized for many years as a source of therapeutic agents and structural diversity (Kingston, 2011; Shen, 2015).

Several studies revealed strong MAO inhibitory activity from herbal sources such as flavonoids, xanthenes, coumarins, caffeine, and alkaloid derivatives, which also became good models for synthetic MAO inhibitors (Erdogan Orhan, 2016). Moreover, it was found that MAO-B inhibitors may as well act as $AA_{2A}R$ antagonists due to the similarity of their binding cavities (Carradori et al., 2014). There is also an increasing body of evidence that safinamide alleviates motor and non-motor PD symptoms through not only MAO-B inhibition which palliates the dopamine deficit in the brain but also by regulating glutamate release through voltage-dependent sodium channels blockade and calcium channels modulation (Stocchi et al., 2022). Furthermore, Ifenprodil, an antagonist of the NMDA receptor, specifically of GluN1 (glycine-binding NMDA receptor subunit 1) and GluN2B (glutamate-binding NMDA receptor subunit 2) subunits was found to possess competitive MAO-A and MAO-B inhibitory activities in the rat brain (Arai et al., 1991). These findings suggest the multi-target potential of these drugs to act on multiple targets implicated in various pathways of PD pathophysiology.

The present study aims to search for novel compounds from NPs to act as multitarget drugs against three important targets for the development of antiparkinsonian drugs: MAO-B, $AA_{2A}R$, and NMDAR. These compounds could potentially provide combined symptomatic relief and neuroprotective activities for patients with PD. A multi-stage virtual

screening approach combining QSAR classification models, pharmacophore screening, molecular docking, and ADME evaluation was conducted to study at the molecular level the interactions of NPs from the COCONUT database, with MAO-B, AA_{2A}R, and NMDAR (Sorokina et al., 2021). The stability of the lead compounds was further assessed through 100 ns molecular dynamics (MD) simulations and compared to the reference drugs. Active site residues and binding pocket of the reference complexes of MAO-B, AA_{2A}R and NMDAR are illustrated in Figure S1 in Supporting Information.

2. Materials and methods

2.1. ML and CNN-based QSAR models

Three bioactivity datasets for each target were retrieved from the ChEMBL database (<https://www.ebi.ac.uk/chembl/>), containing chemical structures and their reported bioactivity against human MAO-B, AA_{2A}R, and NMDAR (GluN1/2B), including 5,066 molecules with reported half maximal inhibitory concentration (IC₅₀) values for hMAO B, 7,813 molecules with reported constant dissociation (*k_i*) values for hAA_{2A}R and 699 reported IC₅₀ for NMDAR (GluN1/2B) belonging to homo sapiens and rattus norvegicus since these two organisms express NMDAR (GluN1/2B) with a percent identity matrix of 98.58% based on UniProt sequence alignment tool (Gaulton et al., 2012; The UniProt Consortium, 2021). The datasets were manually curated, and duplicate compounds were removed by taking the mean value when multiple bioactivity values were reported for a given compound. Logarithmic transformation was applied to all the activity

values to better determine the potency of the compounds using the negative logarithm base 10 scale to represent the data in a more interpretable manner (Tarasova et al., 2015). The compounds were then classified as either active or inactive. An activity value >6.5 was used to label active compounds, whereas all compounds displaying an activity value <5 were labeled as inactive as reported in the literature (Burggraaff et al., 2020). Compounds falling within the intermediate range were omitted from the study. The workflow of QSAR modeling is shown in Figure 1.

All investigated compounds from the final datasets were then converted to SMI (Simplified Molecular Input) format, and RDKit cheminformatics software was used to generate chemical structures as graphs, and then as binary molecular descriptors based on the popular Morgan fingerprints, also known as extended-connectivity fingerprints (ECFP4) (Ding et al., 2021; Landrum, 2013).

Finally, three machine learning classification algorithms, namely Random Forest, Extra Trees, and Support Vector Machine were used to generate QSAR models for the selected targets through Scikit-learn machine learning library in Python (Pedregosa et al., 2011; Wu et al., 2021). Convolutional neural networks (CNNs) are a category of neural networks that have proven very effective in areas such as image recognition and classification (Wang et al., 2021). CNNs generally consist of many convolutional layers and one connected layer corresponding to a classic neural network (Figure S2 in Supporting Information). Graph-based and fingerprint-based CNN models were generated to compare their performance with traditional ML algorithms using Keras and TensorFlow libraries in Python (Singh et al., 2020; Gulli & Pal, 2017).

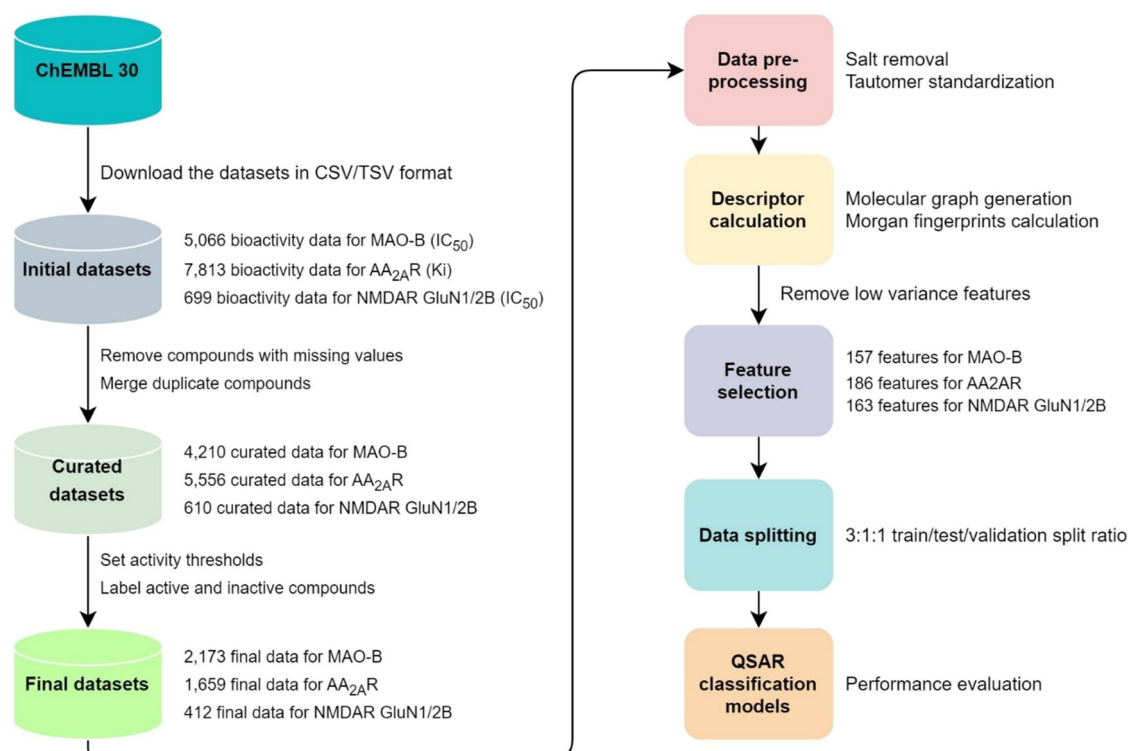


Figure 1. Workflow of QSAR modeling for the prediction of MAO-B, AA_{2A}R, and NMDAR bioactivity.

Datasets were split into training, testing, and validation sets using a 3:1:1 split ratio (Craft & Leake, 2002). The receiving operating characteristic (ROC) curves were used as a quality parameter to assess the performance of the classification models by plotting the true positive rate (sensitivity) against the false negative rate (specificity), the area under the ROC curve (AUC) values range from 0.5 indicating no discrimination to 1 indicating a perfect separation between the two classes (Hanley & McNeil, 1982; Herrera-Acevedo et al., 2021). Performance metrics were calculated such as sensitivity (SEN) Equation (1), specificity (SPC) Equation (2), false positive rate (FPR) Equation (3), false negative rate (FNR) Equation (4), Matthews Correlation Coefficient (MCC) Equation (5), and accuracy (ACC) Equation (6). Five-fold cross-validation using 100 data splits was also used to evaluate the performance of the selected models. Finally, the validation sets that were not presented to the generated QSAR models yet were used for external validation of the developed QSAR classification models.

$$SEN = \frac{TP}{(TP + FN)} \quad (1)$$

$$SPC = \frac{TN}{(FP + TN)} \quad (2)$$

$$FPR = \frac{FP}{(FP + TN)} \quad (3)$$

$$FNR = \frac{FN}{(FN + TP)} \quad (4)$$

$$ACC = \frac{(TP + TN)}{(P + N)} \quad (5)$$

$$MCC = \frac{(TP \times TN) - (FP \times FN)}{\sqrt{(TP + FP) * (TP + FN) * (TN + FP) * (TN + FN)}} \quad (6)$$

SEN: Number of actual positives correctly identified by a classification model; *SPC*: Number of actual negatives correctly identified by a classification model; *FPR*: Number of negatives incorrectly classified as positives by a classification model; *FNR*: Number of positives incorrectly classified as negatives by a classification model; *ACC*: Overall accuracy of a classification model by calculating the ratio of correct predictions to the total number of predictions; *MCC*: is a statistic that quantifies the quality of binary classification results by considering true and false positives and negatives in a single value, ranging from -1 (perfect disagreement) to $+1$ (perfect agreement). *TP*: Number of true positives; *TN*: Number of true negatives; *FP*: Number of false positives; *FN*: Number of false negatives; *P + N*: Total number of a dataset.

2.2. Ligand database preparation

Chemical structures of the NPs were retrieved in SMILES format from the COCONUT database, the largest NPs database to date (Sorokina et al., 2021). Primary filtration was conducted based on Lipinski's rule of five to eliminate all compounds that present any violation of the five rules of orally active drugs (Lipinski, 2004; Pollastri, 2010). 2D chemical structures and physicochemical properties of all the compounds were computed using the DataWarrior Cheminformatics program to

only retain those with values falling in the recommended range (Sander et al., 2015). Possible ionization states were generated for all ligands at physiological pH of 7.0 ± 2.0 using the Ligprep module of Maestro 12.5 and OPLS3e force field (Roos et al., 2019).

2.3. Pharmacophore modeling

Ligand-based virtual screening was conducted using a pharmacophore model generated from the reference NMDAR antagonist, ifenprodil, and an experimentally evaluated compound, *N*-(4-chloro-1H-benzimidazol-2-yl) benzamide, which displayed an inhibitory activity in the nanomolar range for MAO-B and AA_{2A}R (Jaiteh et al., 2018; Williams, 2001). Molecular docking was conducted using Glide Extra Precision (XP) mode to identify bioactive conformations for the dual-target reference ligand and the key moieties responsible for the binding with MAO-B and AA_{2A}R (Friesner et al., 2006). Alternatively, the bioactive conformation of the NMDAR antagonist, ifenprodil was taken from the crystallographic 3D structure from RCSB PDB (<https://www.rcsb.org/>), (PDB ID: 5EWJ) (Stroebel et al., 2016). The alignment of these two ligands was conducted and the Phase module of Maestro 12.5 was used to generate a 3D-pharmacophore model containing the identified pharmacophoric features necessary for the multi-blockade of MAO-B, AA_{2A}R, and NMDAR (Dixon et al., 2006). The developed 3D-pharmacophore model was then used to further filter the NPs and only retain compounds meeting the proposed pharmacophoric criteria.

2.4. Molecular docking

Crystallographic structures of MAO-B (PDB ID: 2V5Z, resolution = 1.7 Å), AA_{2A}R (PDB ID: 5IU4, resolution = 1.7 Å), and NMDAR (PDB ID: 5EWJ, resolution = 2.7 Å) in complex with reference inhibitors, safinamide, ZM-241385, and ifenprodil, respectively, were retrieved from RCSB PDB (<https://www.rcsb.org/>) (Binda et al., 2007; Segala et al., 2016; Stroebel et al., 2016). All the structures were processed using the protein preparation wizard to assign bond orders, add explicit hydrogens to the structure, and fix and optimize side chains missing atoms using Prime (Boulaamane et al., 2023; Jacobson et al., 2002, 2004). Protonation states for the residues were assigned using the PROPKA program for predicting the pK_a of protein residues at pH = 7.0 (Olsson et al., 2011).

Co-crystallized ligands were used for the grid box placing using the receptor grid generation tool (Schrödinger Release 2022-3: Maestro, 2020). Grid dimensions were chosen large enough to dock ligands with a similar size to the reference compounds. Molecular docking was performed using Glide (XP) mode in Maestro 12.5 with a maximum output of five conformations per ligand (Friesner et al., 2006). The best docking poses were chosen according to their docking score and RMSD value towards the native ligand for each target protein.

2.5. ADME properties prediction

Nearly 40% of drug candidates fail in clinical trials due to poor Absorption, Distribution, Metabolism, and Excretion (ADME) properties (Lin et al., 2003). *In silico* ADME prediction is a quick tool to find if a compound is druglike by calculating its pharmacokinetics parameters and physicochemical properties and can considerably reduce the amount of consumed time and resources during the overall drug development process (Bhandari et al., 2022). The selected compounds were analyzed based on common pharmacokinetic parameters including lipophilicity, water solubility, human oral absorption, brain/blood partition coefficient, and human serum albumin binding which were predicted using the Qikprop tool (Ioakimidis et al., 2008). An overview of the virtual screening workflow is represented in Figure S3 in Supporting Information.

2.6. Molecular dynamics simulations

The stability of the most potent compounds complexed with the selected target proteins was evaluated through 100 ns MD simulations using the Desmond module included in Maestro 12.5, Schrödinger's suite (2020-3) (Bowers et al., 2006). The water-soaked solvated system was created in Desmond using the System Builder panel. The OPLS3e force field was selected, and Single Point Charge (SPC) was used as a solvent model with a 10 Å orthorhombic box for both proteins. The system was neutralized by randomly adding enough counter-ions (Na^+ and Cl^-) and an isotonic state was maintained by adding 0.15 M NaCl. The solvated model

system was subjected to energy minimization using OPLS3e force field parameters as the default protocol associated with Desmond (He et al., 2022). Then, the system was equilibrated throughout the simulation time via Constant Number of Particles, Pressure, and Temperature (NPT) ensemble at a constant 300 K temperature and 1 atm pressure using the Nose-Hoover thermostat algorithm and Martyna-Tobias-Klein Barostat algorithm, respectively (Ke et al., 2022). A total of 100 ns simulations were carried out, during which 1000 frames were recorded. Finally, the MD simulation trajectory was analyzed using the Simulation Interaction Diagram (SID) tool (AlAjmi et al., 2018).

3. Results and discussion

3.1. QSAR models validation

The ROC curve was used to assess the quality of the developed QSAR classification models by plotting the true positive rate against the false positive rate. For all the classification models, AUC values greater than 0.80 were achieved for MAO-B, whereas some classification models for AA_{2A}R displayed lower AUC values as illustrated in Figure 2. The performance of all the built QSAR models was evaluated using different performance metrics as shown in Table 1. Similarly, external validation of the developed QSAR classification models is summarized in Table 2.

Based on the performance of the QSAR classification models on internal and external datasets, the Random Forest model was found to perform the best with an AUC value of 0.93, 0.91, and 0.94 and MCC value for external sets of 0.81,

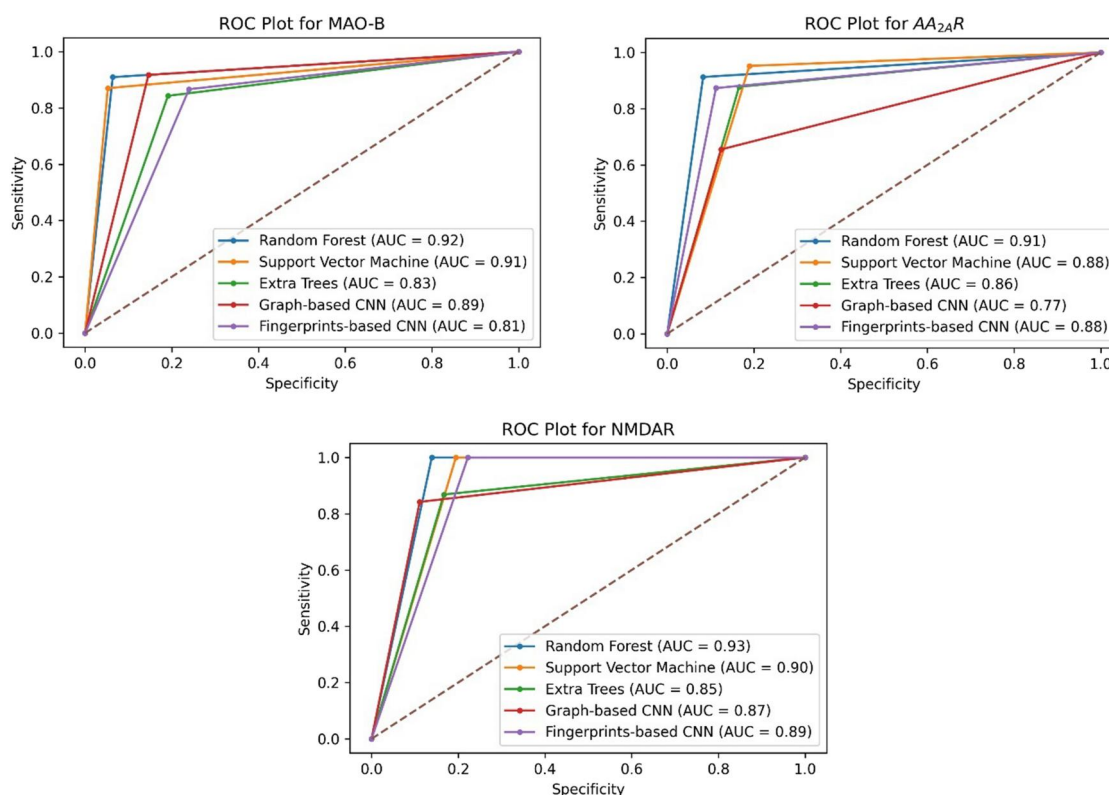


Figure 2. ROC plots of the generated QSAR classification models for MAO-B, AA_{2A}R, and NMDAR.

Table 1. Performance of the developed QSAR classification models.

Target protein	Model	Testing set						5-fold CV
		SEN	SPC	FPR	FNR	MCC	ACC	ACC
MAO-B	Random forest	0.92	0.93	0.06	0.07	0.85	0.92	0.92
	Support vector machine	0.89	0.93	0.20	0.15	0.82	0.91	0.91
	Extra trees	0.84	0.80	0.06	0.10	0.82	0.64	0.84
	Graph-based CNN	0.86	0.76	0.23	0.13	0.63	0.81	0.83
	Fingerprints-based CNN	0.93	0.87	0.12	0.06	0.80	0.90	0.86
AA _{2A} R	Random forest	0.88	0.93	0.06	0.11	0.82	0.91	0.90
	Support vector Machine	0.92	0.87	0.12	0.16	0.77	0.89	0.86
	Extra trees	0.83	0.87	0.12	0.07	0.85	0.71	0.81
	Graph-based CNN	0.65	0.87	0.12	0.34	0.53	0.74	0.74
	Fingerprints-based CNN	0.83	0.92	0.07	0.16	0.76	0.88	0.87
NMDAR	Random forest	0.97	0.90	0.09	0.02	0.88	0.94	0.91
	Support vector machine	0.97	0.87	0.12	0.16	0.84	0.91	0.90
	Extra trees	0.84	0.87	0.12	0.02	0.85	0.71	0.86
	Graph-based CNN	0.84	0.91	0.08	0.15	0.76	0.87	0.88
	Fingerprints-based CNN	0.97	0.86	0.13	0.02	0.82	0.90	0.90

SEN: sensitivity (true positive rate); SPC: specificity (true negative rate); FPR: false positive rate; FNR: false negative rate; MCC: Matthews correlation coefficient; ACC: accuracy; 5-fold CV: 5-fold cross-validation.

Table 2. External validation of the developed QSAR classification models.

Target protein	Model	Performance metrics					
		SEN	SPC	FPR	FNR	MCC	ACC
MAO-B	random forest	0.87	0.93	0.06	0.12	0.81	0.90
	Support vector machine	0.85	0.95	0.15	0.14	0.79	0.89
	Extra trees	0.85	0.84	0.04	0.14	0.84	0.69
	Graph-based CNN	0.81	0.80	0.19	0.18	0.61	0.80
	Fingerprints-based CNN	0.84	0.82	0.17	0.15	0.67	0.83
AA _{2A} R	Random forest	0.92	0.93	0.06	0.07	0.85	0.93
	Support vector machine	1.00	0.83	0.13	0.12	0.78	0.88
	Extra trees	0.87	0.86	0.16	0.00	0.87	0.73
	Graph-based CNN	0.72	0.87	0.12	0.27	0.60	0.80
	Fingerprints-based CNN	0.92	0.88	0.11	0.07	0.79	0.90
NMDAR	Random forest	1.00	0.90	0.10	0.00	0.89	0.94
	Support vector machine	1.00	0.86	0.15	0.06	0.84	0.91
	Extra trees	0.93	0.85	0.14	0.00	0.89	0.78
	Graph-based CNN	0.83	0.88	0.12	0.17	0.72	0.86
	Fingerprints-based CNN	1.00	0.82	0.18	0.00	0.79	0.89

SEN: sensitivity (true positive rate); SPC: specificity (true negative rate); FPR: false positive rate; FNR: false negative rate; MCC: Matthews correlation coefficient; ACC: accuracy.

0.85, and 0.89 for MAO-B, AA_{2A}R, and NMDAR, respectively. The model was then selected for target bioactivity prediction against the selected proteins. Out of 216,115 drug-like compounds, 13,996 were predicted as active for MAO-B, among them 1,106 were active for AA_{2A}R and 354 were predicted as actives for all the selected targets. To avoid chemical sampling bias, a wide chemical space diversity of the training sets is mandatory, and it contributes to high prediction accuracy and strong generalization ability of the classification models (Yang et al., 2022). The chemical space diversity of the curated datasets of the selected targets alongside the predicted active NPs were explored using the t-stochastic neighbor embedding (t-SNE) statistical method (Van der Maaten & Hinton, 2008) as shown in Figure 3. Distinct clusters of active compounds, likely signifying diverse scaffolds and chemotypes targeting the same protein were observed. These clusters are clearly separated from inactive compounds. Interestingly, unique clusters emerge from the screened natural products (NPs), potentially representing novel chemical classes absent in the ChEMBL datasets. These NP clusters also exhibit clear separation from inactive compounds (Figure 2).

3.2. Pharmacophore screening

The pharmacophore hypothesis was based on an experimentally validated MAO-B inhibitor/AA_{2A}R antagonist, and on ifenprodil, an NMDAR antagonist as shown in Figure 4(A,B), respectively. The molecular docking study revealed the importance of the nitrogen atom of the furan and the benzene ring to act as a hydrogen bond donor and establish a hydrogen bond with a key residue in the MAO-B entrance cavity of the active site namely Tyr-326. This residue is specific to the MAO-B isoform and acts as a gating residue to allow the binding of selective MAO-B inhibitors (Binda et al., 2011; Milczek et al., 2011). Moreover, this same component is also responsible for the hydrogen bonding with Asn-253 of the active site of AA_{2A}R, a key interaction deemed important for the stability of AA_{2A}R antagonists (Jaakola et al., 2010). In NMDAR, the nitrogen atom is responsible for forming a hydrogen bond with Gln-110B as reported in the literature (Fjellidal et al., 2019). The 3D-pharmacophore model generated using the Phase module consisted of two aromatic rings separated by a distance of 11 Å as shown in Figure 4(C) reflecting the length of the

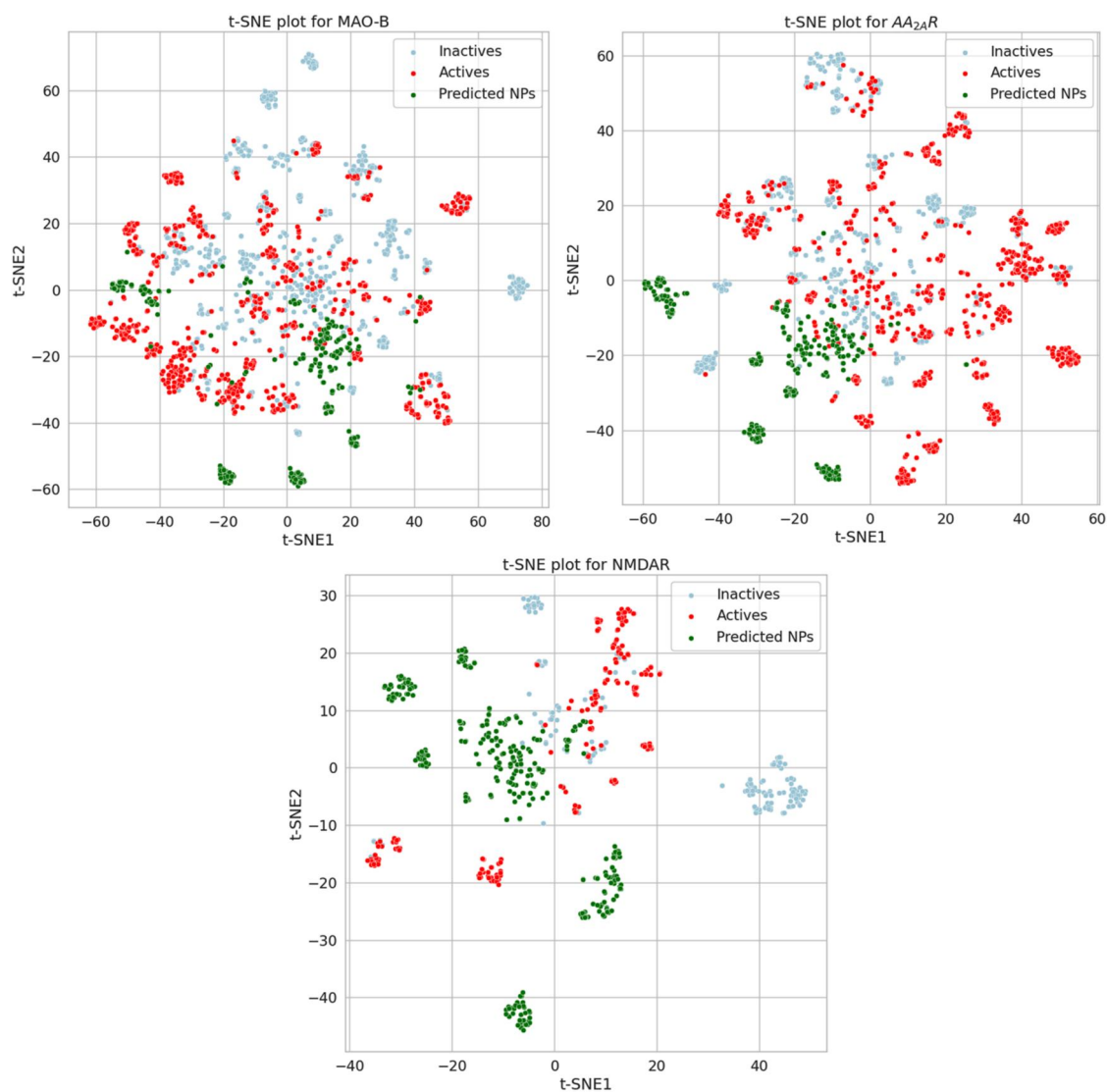


Figure 3. Visual representation of curated ChEMBL datasets for MAO-B, AA_{2A}R, and NMDAR, alongside the predicted active NPs from the QSAR screening using t-SNE method based on Morgan fingerprints.

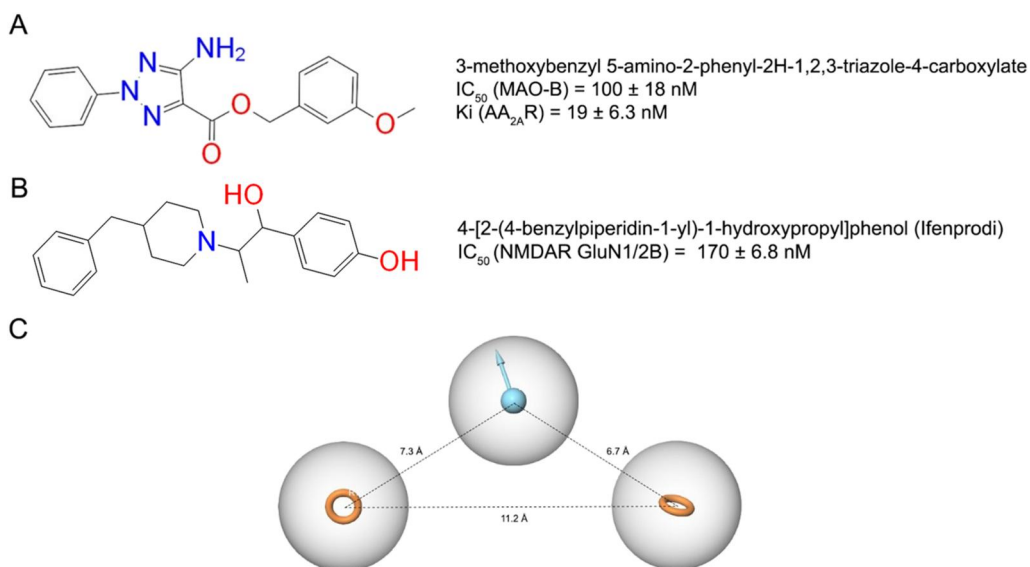


Figure 4. (A) Chemical structure and experimental values of the reference dual MAO-B/AA_{2A}R ligand; (B) chemical structure of the NMDAR reference antagonist, ifenprodil; (C) proposed 3D-pharmacophore model to screen for multi-target drugs, the hypothesis consisted of three pharmacophoric features: one aromatic ring, one hydrogen bond donor, and one aromatic ring.

binding site cavities of the selected targets, and one donor group in the middle which is deemed important for establishing conventional hydrogen bonds with Tyr-326, Asn-253, and Gln-110B of MAO-B, AA_{2A}R, and NMDAR active site, respectively.

3.3. Molecular docking results

The docking protocol implemented in the Glide module was validated by redocking the crystal ligands of human MAO-B, AA_{2A}R, and NMDAR (GluN1/2B). Native ligands were downloaded from the PubChem database with the following CIDs: 131682 for safinamide, 176407 for ZM-24138, and 3689 for ifenprodil (Kim et al., 2021). The Ligprep module was employed for energy minimization using default settings. The root-mean-square deviation (RMSD) was calculated by superposing both docked and native ligands. The results yielded values of 0.12, 0.83, and 0.88 Å for MAO-B, AA_{2A}R, and NMDAR which indicates a good accuracy of the docking program (Figure S4 in Supporting Information). The prepared and filtered compounds were initially screened using the generated pharmacophore model to remove the compounds that do not match the selected pharmacophoric sites. At this stage, 22 of 354 ligands were retained. Subsequently, molecular docking was conducted on the remaining compounds against MAO-B, AA_{2A}R and NMDAR active sites using Glide Extra Precision (XP) mode (Friesner et al., 2006). The chemical structures of the remaining compounds are shown in Figure 5. The docking scores and protein-ligand

interactions are shown in Table 3. The selected binding poses of the two highest-ranking compounds with the selected targets are shown in Figure 6. The chemical space of the 22 compounds highlighting the top two lead compounds, was visualized using t-SNE plots to assess their positioning relative to the reference compounds (Figure S5 in Supporting Information). The two lead compounds exhibited very close proximity, indicating a high degree of similarity. Additionally, in the AA_{2A}R plot, the compounds overlapped with the reference active compounds. However, no similar active compounds were identified in the MAO-B and NMDAR datasets, implying the novelty of these drugs and the need for *in vitro* testing.

3.4. ADME evaluation results

ADME properties results for the selected NPs are shown in Table 4. Qikprop predicted aqueous solubility shows that all the compounds have values within the recommended range (−6.5 to 0.5) where 95% of similar values for known drugs fall inside. Predicted human oral absorption shows that most of the natural compounds have better oral absorption than the reference ligands, and thus greater bioavailability. Brain/blood partition coefficient (QPlogBB) was also predicted, all the values are within the range of recommended values for compounds that penetrate the blood-brain barrier (−3.0 to 1.2) (Boulaamane et al., 2022). Caco-2 cells are a good mimic for the gut-blood barrier, predicted apparent Caco-2 cell permeability cell is considered great if >500 and

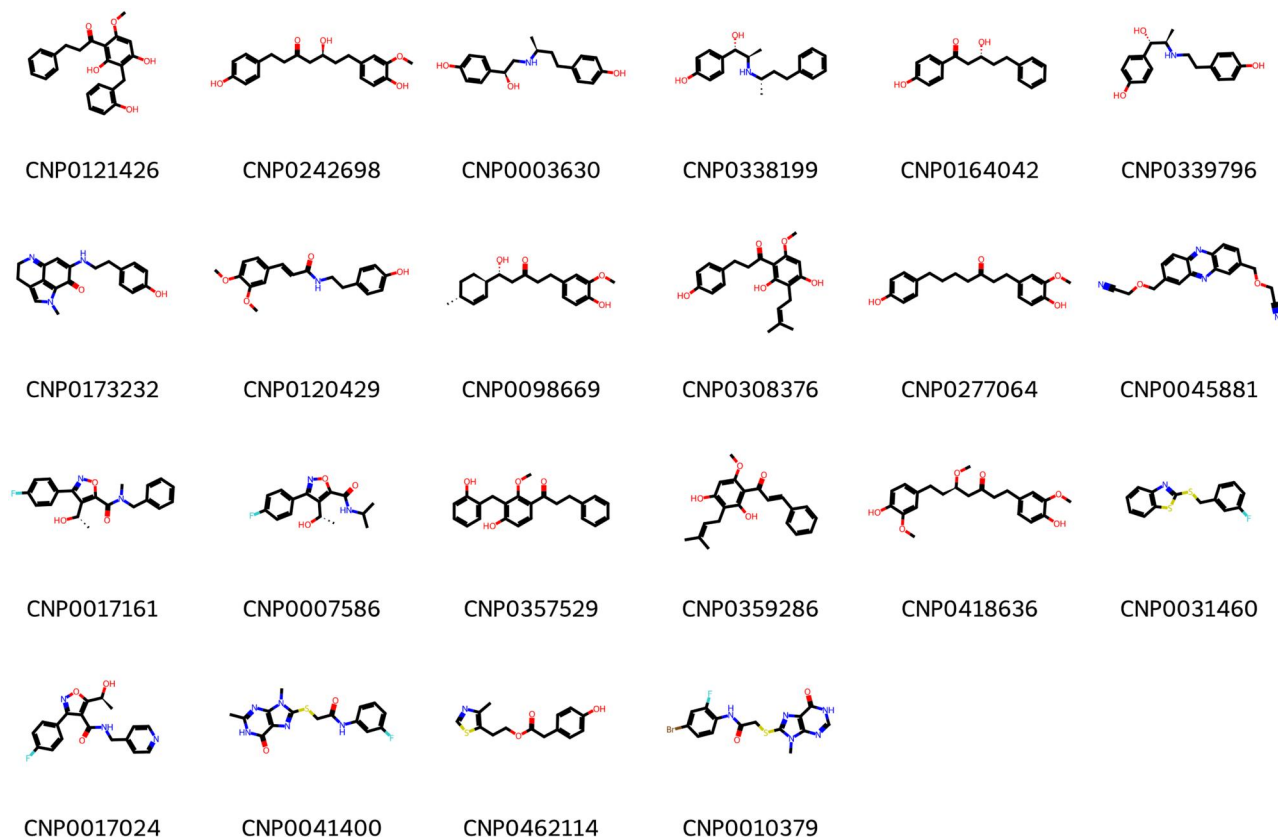
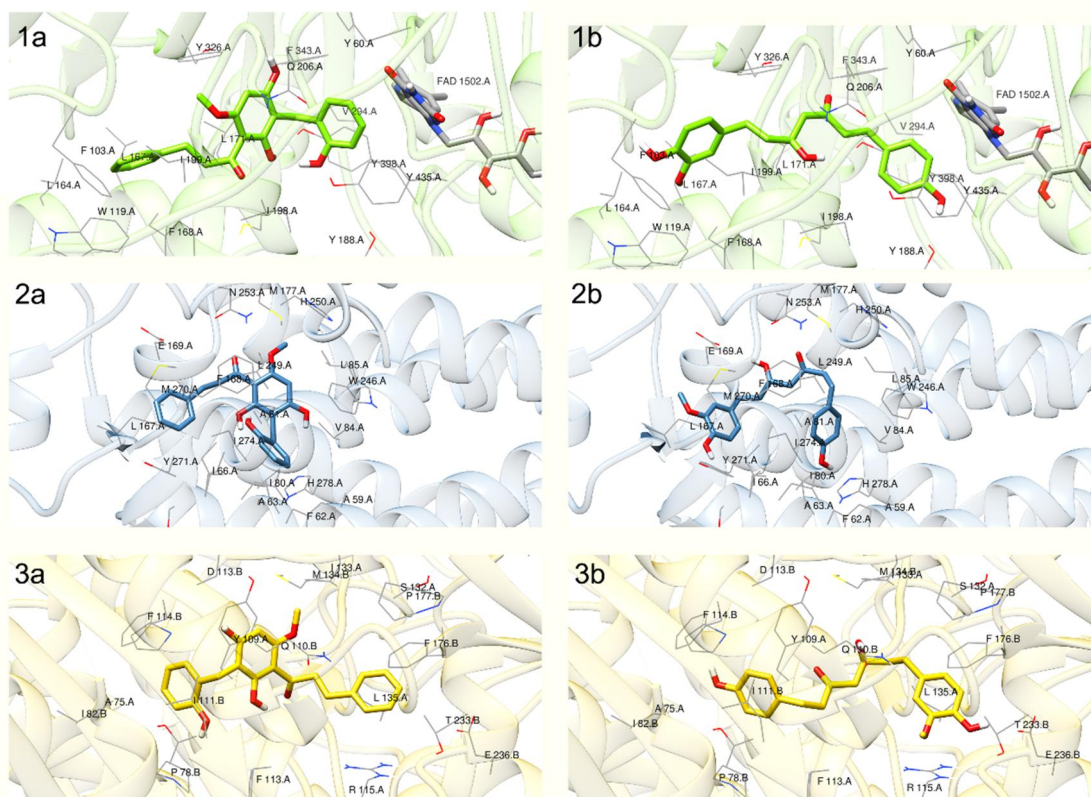


Figure 5. Chemical structures of the remaining 22 compounds selected for molecular docking against MAO-B, AA_{2A}R, and NMDAR.

Table 3. Molecular docking results of the retained NPs against MAO-B, AA_{2A}R, and NMDAR.

Compound	Glide XP score (kcal/mol)			Hydrogen bonds			π-π interactions		
	MAO-B	AA _{2A} R	NMDAR	MAO-B	AA _{2A} R	NMDAR	MAO-B	AA _{2A} R	NMDAR
Safinamide	-11.5	-9.1	-9.5	Gln-206	Glu-169	Asp-113BAsp-136B	Tyr-326	—	Tyr-109APhe-114B
ZM-241385	-9.9	-10.8	-9.4	Cys-172Tyr-188	Glu-169Asn-253	Tyr-110Alle-133A	Tyr-326	Phe-168Hid-250	Tyr-109A
Ifenprodil	-7.7	-6.5	-11.2	Cys-172Tyr-188	Tyr-271	Gln-110BGlu-236B	—	Hid-250	Phe-114BPhe-176B
CNP0121426	-12.0	-12.4	-10.0	Leu-171	Asn-253	Gln-110B	Phe-168Tyr-326	—	Tyr-109APhe-176B
CNP0242698	-12.4	-11.4	-9.5	Ile-198Gly-434	Asn-253Ile-66	Gln-110BArg-115AGlu-236B	Tyr-398Tyr-435	—	Phe-114BPhe-176B
CNP0003630	-10.9	-9.3	-9.3	Ile-198Gly-434Tyr-435	Phe-168Ile-66Ile-80	Gln-110BGlu-236B	Tyr-435	—	Phe-176B
CNP0338199	-10.6	-9.1	-9.0	Ile-199	Asn-253Ala-63	Tyr-109A	—	Phe-168	—
CNP0164042	-9.1	-10.3	-9.0	Ile-198Tyr-435	Glu-169Tyr-271	Gln-110BGlu-236B	Tyr-435	—	Phe-176B
CNP0339796	-8.4	-8.6	-11.1	Ile-198	Asn-253Ile-66	Tyr-109AThr-110A	—	—	—
CNP0173232	-10.4	-9.8	-7.4	Tyr-398	Glu-169Asn-253	Thr-110Alle-133AGln-110B	Tyr-326Tyr-398	Phe-168	Tyr-109A
CNP0120429	-9.7	-8.9	-8.9	Gly-434	—	Gln-110BGlu-236B	Tyr-435	Tyr-271	Phe-176B
CNP0098669	-9.4	-9.7	-8.4	—	Asn-253	Gln-110B	—	Phe-168	Tyr-109A
CNP0308376	-9.6	-9.3	-8.6	—	Ile-80Glu-169	Tyr-109AGln-110B	Tyr-398	Phe-168	Tyr-109A
CNP0277064	-9.8	-9.3	-8.3	Pro-102Gly-434	Asn-253	Glu-106BThr-110A	Tyr-398	—	—
CNP0045881	-9.6	-11.4	-6.5	Gln-65	Asn-253	—	Tyr-326	Phe-168	Tyr-109A
CNP0017161	-10.2	-8.6	-8.5	—	Ile-66Phe-168Glu-169	Gln-110B	—	—	Phe-114B
CNP0007586	-9.2	-9.6	-8.5	—	Asn-253	Gln-110B	Tyr-326	Phe-168	—
CNP0357529	-9.8	-8.8	-8.6	—	Glu-169	Ser-132A	—	Phe-168	—
CNP0359286	-9.7	-8.9	-8.5	—	Asn-253	Gln-110B	—	—	Tyr-109A
CNP0418636	-10.0	-7.5	-9.0	Gly-434Tyr-435	—	—	Tyr-326	Phe-168Tyr-271	Tyr-109A
CNP0031460	-9.2	-8.9	-7.8	—	Asn-253	—	—	Phe-168	Tyr-109APhe-114B
CNP0017024	-7.3	-9.1	-8.9	Gln-206	—	Gln-110B	Tyr-326	Phe-168	Tyr-109A
CNP0041400	-8.6	-7.2	-7.5	—	Asn-253	Glu-236B	Trp-119	—	Phe-176B
CNP0462114	-7.1	-7.2	-6.5	—	Asn-253	Thr-110A	—	Phe-168	—
CNP0010379	-5.8	-8.0	-5.8	—	Asn-253	Gln-110B	Tyr-326	—	Phe-176B


Figure 6. Selected binding conformations of the most potent multi-target ligands: CNP0121426 (a) and CNP0242698 (b) with MAO-B (1), AA_{2A}R (2), and NMDAR (3).

poor if <25. The predicted QPPCaco values show that most compounds have medium-good Caco-2 cell permeability. Finally, the prediction of binding to human serum albumin

(QPlogKhsa) yielded values for the studied compounds within the recommended range (-1.5 and 1.5) for 95% of known drugs.

Table 4. ADME prediction results of the retained NPs from the Hybrid virtual screening study.

Compound	QLogPo/w	QLogS	%HOA	QLogBB	QPPCaco	QPlogKhsa
Safinamide	1.9	-2.1	76.2	-0.4	112.5	-0.2
ZM-241385	1.6	-4.0	73.3	-1.9	108.7	-0.2
Ifenprodil	3.7	-3.9	95.0	-0.3	392.8	0.5
CNP0121426	4.2	-6.3	100.0	-1.1	760.0	0.5
CNP0242698	3.4	-4.9	87.7	-2.1	188.0	0.3
CNP0003630	2.5	-2.9	74.9	-1.2	75.4	-0.1
CNP0164042	3.5	-4.0	95.9	-1.2	526.0	0.2
CNP0338199	3.2	-3.2	90.5	-0.5	321.8	0.2
CNP0173232	3.2	-4.7	100.0	-0.9	791.1	0.3
CNP0339796	1.6	-2.6	71.8	-1.0	93.7	-0.2
CNP0120429	3.7	-4.6	100.0	-0.9	1256.8	0.3
CNP0098669	3.9	-5.1	100.0	-1.3	654.6	0.5
CNP0308376	4.0	-4.5	100.0	-1.2	592.7	0.5
CNP0277064	3.9	-5.2	96.2	-1.7	389.7	0.4
CNP0045881	1.2	-3.6	75.6	-1.8	204.7	-0.9
CNP0017161	3.2	-4.4	100.0	-0.6	862.1	0.2
CNP0007586	2.8	-4.3	96.8	-0.6	952.2	0.0
CNP0357529	4.1	-4.7	100.0	-0.9	1146.7	0.6
CNP0359286	4.8	-5.3	100.0	-0.9	1294.1	0.8
CNP0418636	3.9	-5.3	100.0	-1.7	539.3	0.3
CNP0031460	4.9	-5.3	100.0	0.5	6952.4	0.6
CNP0017024	2.4	-4.0	88.4	-0.9	462.7	-0.1
CNP0041400	2.1	-4.8	83.6	-1.2	297.8	-0.1
CNP0462114	3.0	-4.3	94.3	-0.9	621.4	0.1
CNP0010379	2.3	-5.0	84.6	-1.0	292.2	-0.1

QLogPo/w: Predicted octanol/water partition coefficient. QLogS: Predicted water solubility; %HOA: Percentage of human oral absorption; QLogBB: Predicted brain/blood partition coefficient; QPPCaco: Predicted apparent Caco-2 cell permeability in nm/sec; QPlogKhsa: Prediction of binding to human serum albumin.

3.5. Molecular dynamics simulations

The results obtained from the molecular docking study could be further validated using MD simulations to assess the stability of the selected NPs under dynamic conditions. Therefore, to further validate the docking results, CNP0121426 and CNP0242698 in complex with MAO-B, AA_{2A}R, and NMDAR were subjected to 100 ns MD simulations and compared to the reference ligands, safinamide, ZM-241385, and ifenprodil under the same conditions. Several parameters including root mean square deviation (RMSD) of C_α atoms, ligand RMSD with respect to protein, root mean square fluctuation (RMSF) of C_α atoms of the proteins, and protein-ligand interactions were analyzed from the MD simulation trajectories.

3.5.1. Root-mean square deviation

In Figure 7, the RMSD plots for the chosen compounds and reference ligands bound to MAO-B, AA_{2A}R, and NMDAR are presented. RMSD values indicate the degree of movement exhibited by the protein and ligand from their original positions, and hence, the stability of the complex. Notably, the CNP0121426-MAO-B complex demonstrated high RMSD values of C_α atoms, reaching approximately 4.8 Å, while CNP0242698-MAO-B remained stable at around 3 Å by the last 50 ns in similar manner to the reference complex. The ligand RMSD for the reference inhibitor, safinamide was stabilized at 1.2 Å as demonstrated in previous studies (Kurczab et al., 2018). Meanwhile, a higher deviation was observed for CNP0121426 reaching 1.8 Å, while CNP0242698 was stabilized at 2.5 Å. The significant variations observed can be attributed to the remarkable flexibility of CNP0242698, which possesses rotatable bonds that impact the ligand's ability to undergo conformational changes to find the optimal binding pose.

Regarding the reference structure of AA_{2A}R, the C_α atoms exhibited RMSD value of 4.8 Å, whereas CNP0121426 and CNP0242698 showed a more stable RMSD at 4 and 3 Å, respectively. However, the reference antagonist ZM-241385 demonstrated a consistent RMSD of approximately 0.6 Å, while CNP0121426 and CNP0242698 displayed a deviation of 6 Å. The increased variances observed can be explained by the expansive binding pocket of AA_{2A}R, which permits the smaller ligands to undergo diverse conformations throughout the simulation period.

In the case of NMDAR, the three protein-ligand complexes exhibited comparable deviations, ranging from 2 to 3.5 Å, consistent with the findings reported in the literature (Touati et al., 2023). Specifically, the CNP0121426 and CNP0242698 complexes had slightly higher deviations of 3.2 and 3.5 Å, respectively. In contrast, the antagonist ifenprodil demonstrated remarkable stability, exhibiting deviations of less than 1.0 Å when bound to both chains A and B of NMDAR. However, CNP0121426 showed larger deviations of 6 Å, while CNP0242698 exhibited stabilized RMSD values at 1.5 Å, which are considered acceptable for lead compounds.

3.5.2. Root-mean square fluctuation

The RMSF is a useful analytical tool for observing atomic fluctuations in protein chains during MD simulations (Benson & Daggett, 2012). Figure 8 displays RMSF plots that highlight areas of the protein that experience the most movement, with peaks indicating high levels of fluctuation. It is common for the N-terminal and C-terminal ends of the protein to exhibit greater fluctuation compared to other regions. Secondary structure elements, such as α-helices and β-strands, tend to be more rigid and less flexible than loop regions, resulting in lower levels of fluctuation. In Figure 9, the MAO-B

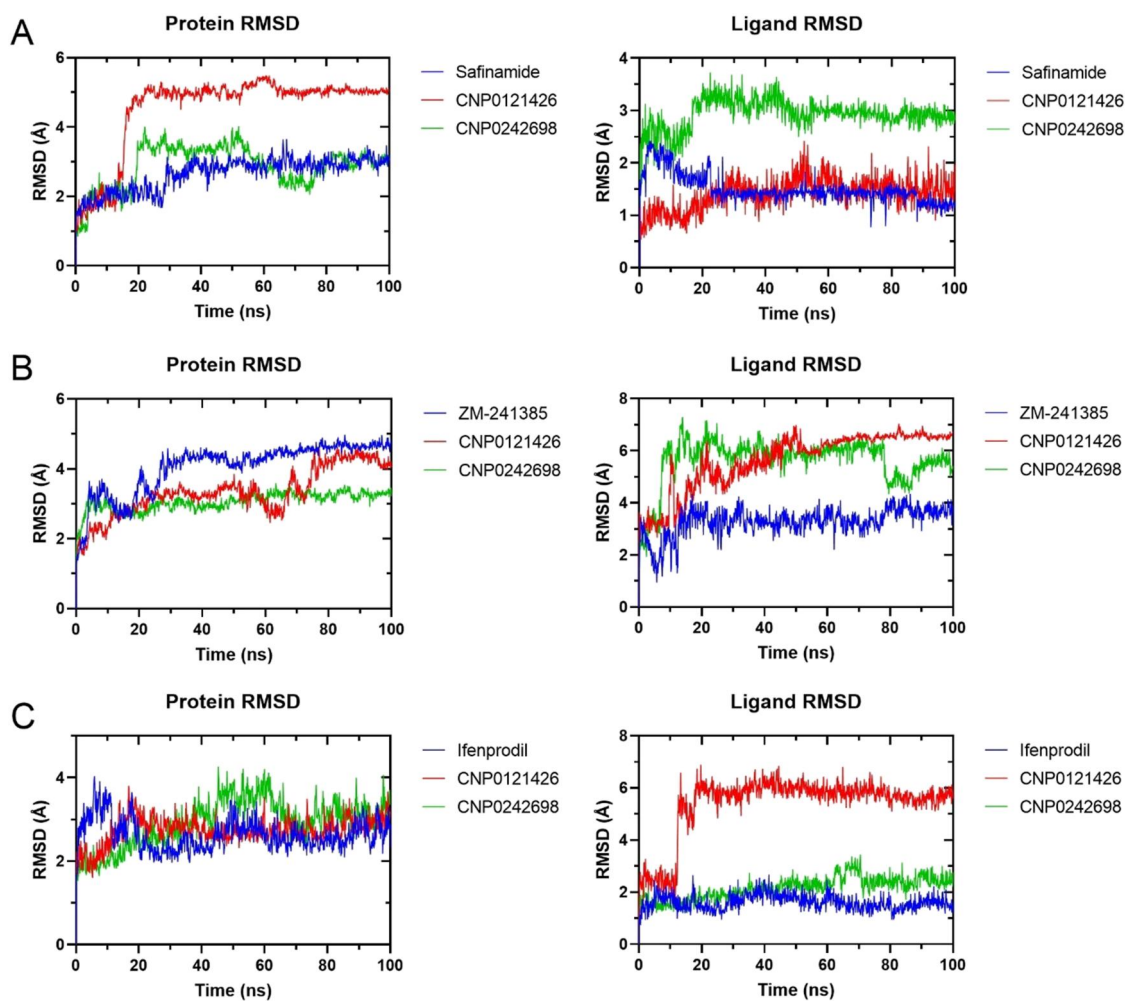


Figure 7. RMSD analysis of C_{α} atoms (Left) and the corresponding ligands (right) of the selected targets: MAO-B (a), AA_{2A}R (B), and NMDAR (C) in complex with the reference ligands, CNP0121426, and CNP0242698.

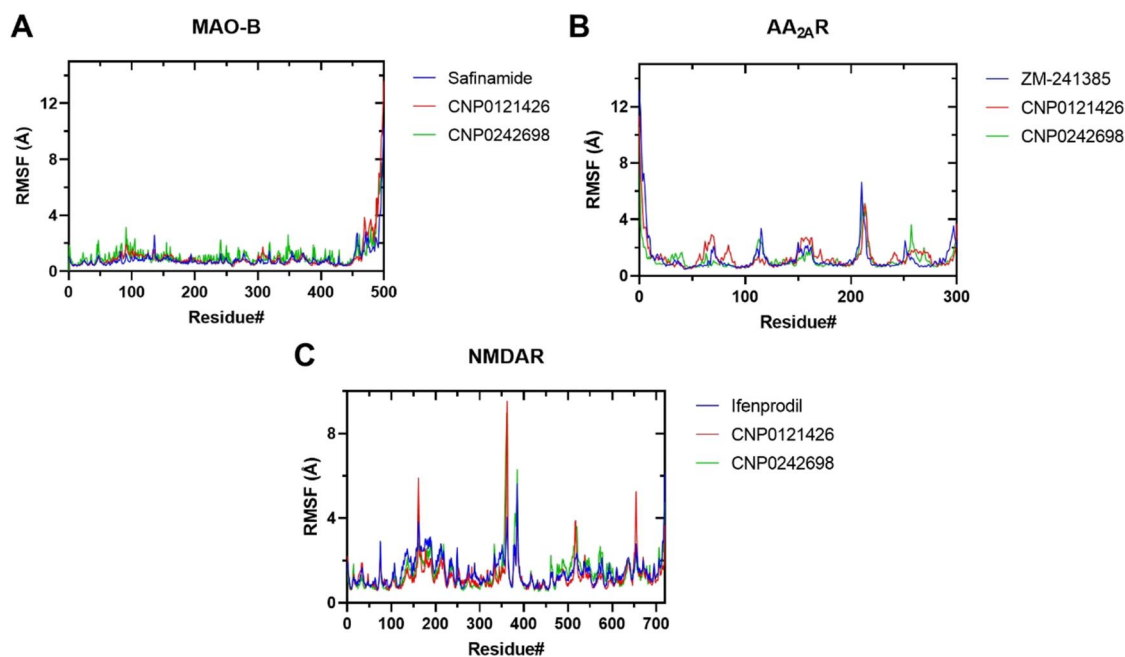


Figure 8. RMSF plots of the selected targets: MAO-B (A), AA_{2A}R (B), and NMDAR (C) in complex with the reference ligands, CNP0121426, and CNP0242698.

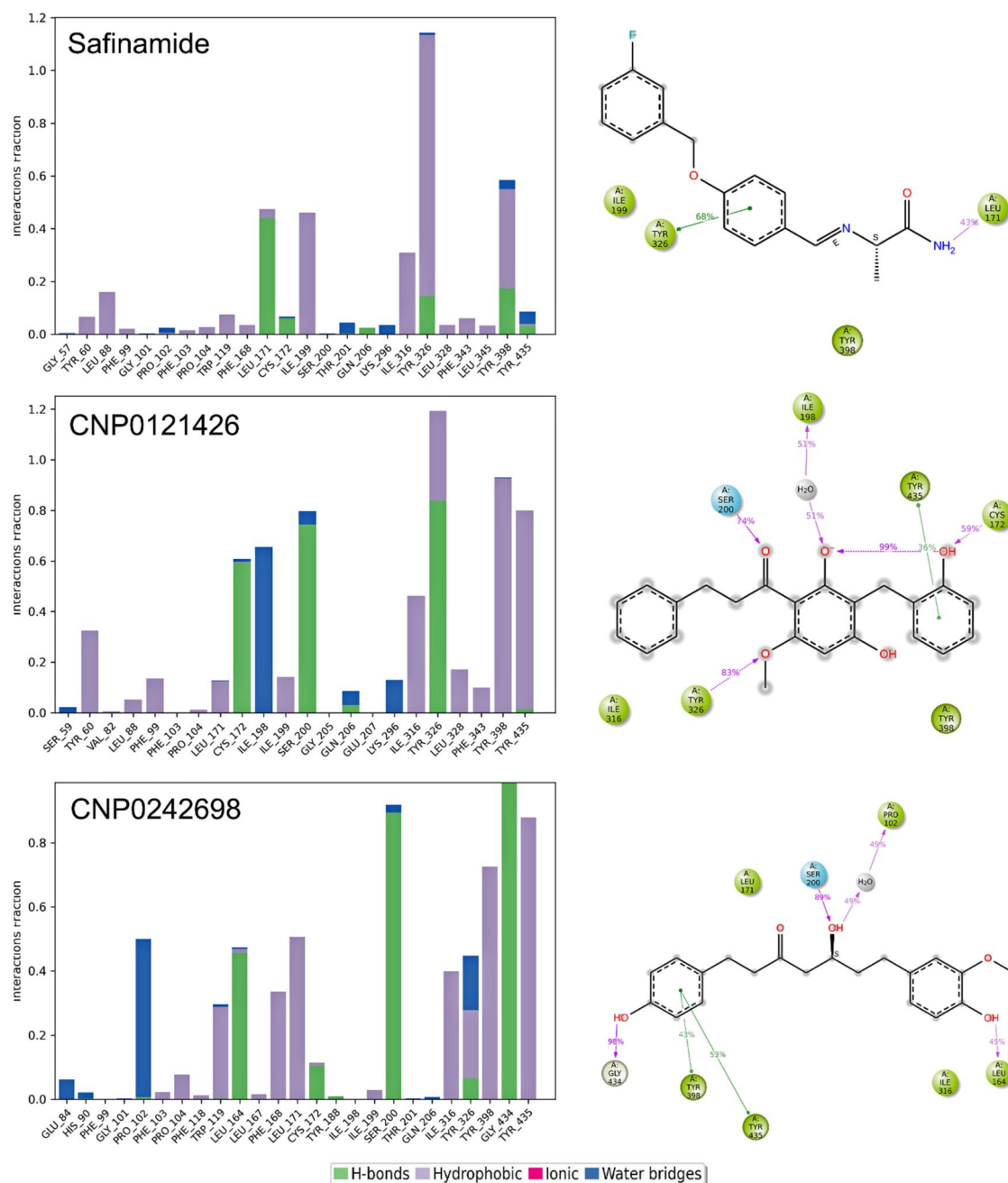


Figure 9. Protein-ligand interaction histograms of safinamide, CNP0121426, and CNP0242698 in complex with MAO-B displaying the fraction of interactions with active amino acids. On the right, schematic representations of the ligands with the percentage of interactions with the protein residues.

enzyme's residues remained consistently stable when bound to the selected compounds, with all fluctuations remaining below 2 \AA during the simulation. The study revealed that the highest level of fluctuation observed in all three MAO-B complexes was at 14 \AA . However, these residues were not involved in ligand binding, as they were in the C-terminal region. This indicates a slight conformational change in the enzyme rather than any significant impact on ligand binding.

The RMSF analysis of AA_{2A}R revealed significant fluctuations of approximately 4.8 \AA in certain regions. Specifically, residues 210–230 showed high flexibility in all three complexes, which is consistent with findings in the literature (Ng et al., 2013). However, the ligand-binding regions experienced less fluctuation, with values of around 2.4 \AA in the reference and CNP0121426 complex. In contrast, the same

region exhibited higher fluctuations in the CNP0242698 complex, indicating a potential conformational change due to the ligand's mode of binding.

In the case of NMDAR, the RMSF analysis highlighted high fluctuations of approximately 5 \AA in certain regions that were not involved in ligand binding. However, the amino acids within the binding site that made contact with the ligands experienced much lower levels of fluctuation, approximately 1.6 \AA , indicating excellent stability of the ligands within their respective binding cavities in all complexes.

3.5.3. Protein-ligand interactions

The role of each amino acid in protein-ligand interactions was unveiled by the simulation results. Figure 9 displays the diagrams

of the molecular interactions with MAO-B, indicating that most of the interactions with the active site of MAO-B are hydrophobic. In the reference complex, Leu-171 formed one preserved hydrogen bond. Due to the hydrophobic nature of the cavity, most other interactions were also hydrophobic. The crucial hydrophobic interactions were primarily formed by Ile-199 and Tyr-326, which serve as the gating residues responsible for substrate and inhibitor specificity (Boulaamane et al., 2023; Milczek et al., 2011). In addition, CNP0121426 formed hydrogen bonds with Cys-172, Ser-200, and Tyr-326. The simulation also highlighted the presence of strong water bridges involving Ile-198. Furthermore, CNP0242698 mainly interacted with Ser-200 and Gly-434 through hydrogen bonds. Other hydrophobic interactions with Ile-316, Tyr-398, and Tyr-435 of the aromatic cage were also observed.

Figure 10 displays the protein-ligand interactions for AA_{2A}R. The simulation results confirm the presence of a

strong hydrogen bond involving Asn-253 between the antagonist ZM-241385 and AA_{2A}R, consistent with previous literature (Welihinda et al., 2016). Additionally, another hydrogen bond involving Ala-63 was identified, along with several hydrophobic interactions involving Phe-168, Leu-249, and His-250. In the case of CNP0121426, a hydrogen bond was observed involving Glu-169, and significant hydrophobic interactions were identified with Phe-168 and His-264. However, CNP0242698 exhibited a greater number of interactions, including hydrogen bonds and water bridges with Ala-59, Ile-80, Val-84, His-250, and Asn-253.

Figure 11 illustrates the highlighted interactions between NMDAR and the selected compounds. As per the literature, the reference antagonist consistently binds with B:Gln-110 via hydrogen bonding (Kumar & Patnaik, 2016), while additional hydrogen bonds are observed with B:Glu-106 and B:Glu-236. Several hydrophobic interactions were also

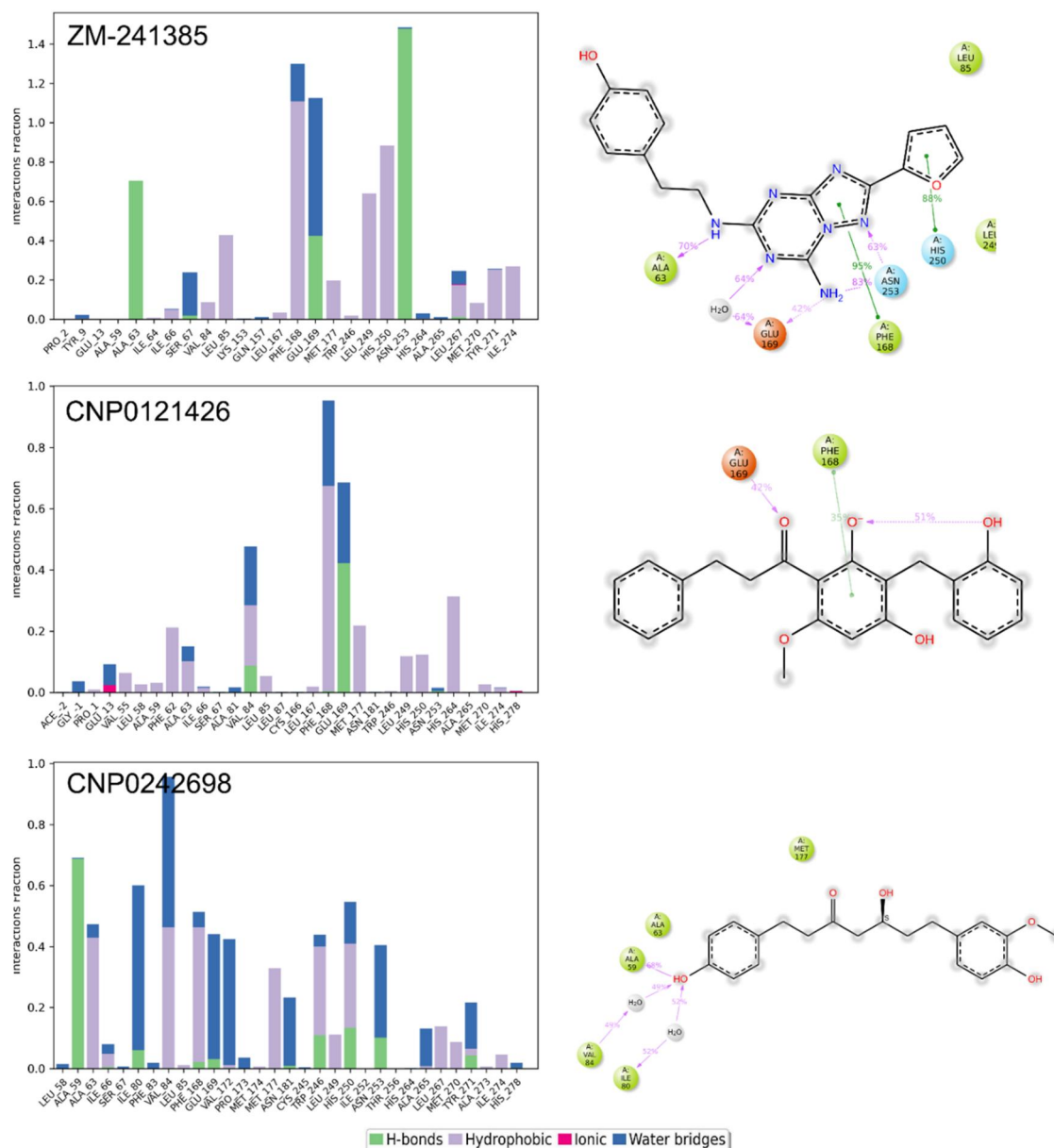


Figure 10. Protein-ligand interaction histograms of ZM-241385, CNP0121426, and CNP0242698 in complex with AA_{2A}R displaying the fraction of interactions with active amino acids. On the right, schematic representations of the ligands with the percentage of interactions with the protein residues.

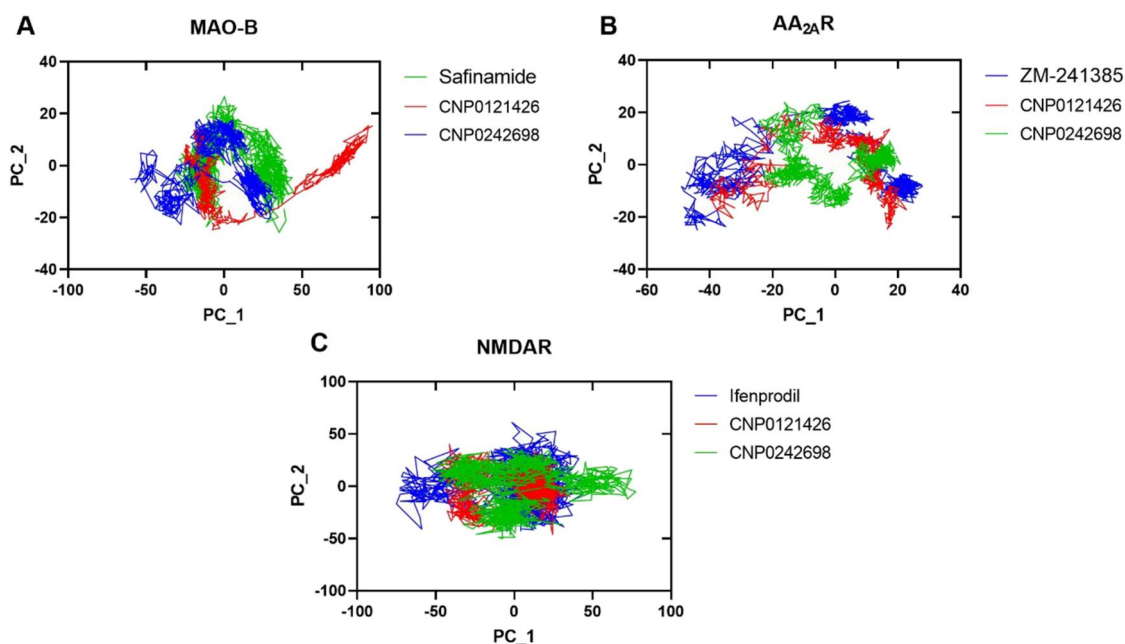


Figure 12. PCA plots for the MD simulations trajectories for MAO-B (A), AA_{2A}R (B), and NMDAR (C) in complex with the reference ligands, CNP0121426, and CNP0242698.

Table 5. Post-MD simulation binding free energy components of the selected protein-ligand complexes calculated using MM-GBSA approach.

Protein-ligand complexes		MM-GBSA (kcal/mol)				
		ΔG_{Bind}	ΔG_{Coul}	ΔG_{Hbond}	ΔG_{Lipo}	ΔG_{vdW}
MAO-B	Safinamide	-137.90 ± 6.43	0.97 ± 27.32	-13.50 ± 0.66	-30.65 ± 0.92	-119.10 ± 3.72
	CNP0121426	-139.43 ± 7.23	-2.78 ± 15.27	-11.11 ± 0.43	-31.09 ± 1.41	-111.89 ± 4.01
	CNP0242698	-147.29 ± 4.36	-5.03 ± 21.27	-11.84 ± 0.51	-31.74 ± 0.93	-119.07 ± 2.47
AA _{2A} R	ZM-241385	-61.80 ± 3.61	-12.01 ± 2.26	-0.99 ± 0.23	-18.64 ± 0.84	-49.32 ± 1.84
	CNP0121426	-59.24 ± 3.45	-5.68 ± 2.54	-0.15 ± 0.23	-13.71 ± 1.37	-48.06 ± 3.62
	CNP0242698	-63.92 ± 3.22	-6.24 ± 1.81	-0.02 ± 0.05	-19.14 ± 1.41	-43.62 ± 2.32
NMDAR	Ifenprodil	-36.87 ± 0.34	-24.72 ± 0.23	-3.94 ± 0.12	-4.52 ± 0.28	-32.17 ± 0.41
	CNP0121426	-35.72 ± 0.27	-22.48 ± 0.31	-2.02 ± 0.17	-5.74 ± 0.25	-29.08 ± 0.37
	CNP0242698	-38.98 ± 0.33	-26.19 ± 0.28	-4.79 ± 0.15	-4.39 ± 0.34	-34.65 ± 0.33

ΔG_{Bind} : free energy of binding; ΔG_{Coul} : Coulomb energy; ΔG_{Hbond} : hydrogen bonding energy; ΔG_{Lipo} : hydrophobic energy; ΔG_{vdW} : Van der Waals energy.

exhibiting a non-stable cluster correspond to less stable complexes. In MAO-B, CNP0242698 displayed conformational motions that followed a similar trend to the reference complex. On the other hand, in AA_{2A}R, CNP0121426 showed the closest resemblance in terms of conformational changes to the reference complex. However, in NMDAR, CNP0121426 exhibited the narrowest range of motions, followed by the reference complex and CNP0242698.

3.5.5. MM-GBSA binding free energy calculation

We conducted MM-GBSA-based binding free energy calculations using the pose viewer file of the docked complexes, and the results are presented in Table 5. The binding free energy values reached values of -147.29 , -63.92 and -38.98 kcal/mol for MAO-B, AA_{2A}R, and NMDAR, respectively. To assess the binding vigor of MAO-B with safinamide, CNP0121426, and CNP0242698, we further decomposed the MM-GBSA binding energies into individual components. It was observed that Van der Waals binding energy played a significant role in the three compounds' interaction with MAO-B, with average binding free energy values of -119.1 , -111.9 , and -119.1 kcal/mol, respectively. Regarding

AA_{2A}R, the calculated ΔG_{bind} values for CNP0121426 (-59.24 kcal/mol) and CNP0242698 (-63.92 kcal/mol) were in close proximity, consistent with the earlier molecular docking findings. In the case of NMDAR, CNP0121426 (-35.72 kcal/mol) and CNP0242698 (-38.98 kcal/mol) exhibited similar results to the reference antagonist, ifenprodil. Notably, electrostatic interactions (Coulomb energy) and Van der Waals forces emerged as significant contributors to ligand binding, as indicated by the high ΔG values.

4. Conclusion

Multitargeting strategies are emerging as a promising approach for the management of neurodegenerative diseases. The current study introduces a novel approach integrating data-driven drug discovery and molecular modeling to screen for potential multi-target compounds from the largest available NPs database. QSAR models were developed for three pivotal targets in PD: MAO-B, AA_{2A}R, and NMDAR. Subsequently, we used the best models for each target to predict the bioactivity of the NPs. The predicted active compounds were then subjected to pharmacophore screening

and molecular docking. Two natural lead candidates, CNP0121426 and CNP0242698, belonging to the dihydrochalcones and curcuminoids chemical classes, respectively, exhibited the highest compound rankings. Further structural analysis revealed favorable interactions within the binding sites of all three targets. The stability of the lead candidates in complex with the selected targets was further assessed through MD simulations. Despite the high RMSD with respect to the protein, curcuminoid demonstrated improved stability in the case of MAO-B. Similarly, the structure of AA_{2A}R complexed with the curcuminoid exhibited higher stability compared to the reference complex. However, the inherent flexibility of the ligand resulted in higher ligand RMSD initially, which eventually stabilized by the end of the simulation, suggesting that it requires more time to accommodate an optimal orientation within the binding pocket. In NMDAR, although more protein deviations were observed, curcuminoid, CNP0242698 exhibited good stability compared to the dihydrochalcone ligand. Overall, the curcuminoid complexed with the studied structures displayed superior stability compared to the dihydrochalcone, indicating its potential as a multitarget agent in combating PD. Results obtained from the current study may generate an increased shift of interest toward developing novel antiparkinsonian drugs with neuroprotective activities from NPs. However, additional experimental studies are needed to further validate these findings.

We would like to thank Prof. Francisco Javier Luque Garriga, University of Barcelona, Spain, for his constructive criticism and Dr. Pankaj Mishra, Neovarsity, Germany for his invaluable knowledge in machine learning and artificial intelligence. Their contribution is sincerely appreciated and gratefully acknowledged. The authors also acknowledge ProteinsInsights, Nangal Raya, New Delhi, India, for providing computational resources essential for the successful completion of this research work. The authors received no financial support for the research, authorship, and/or publication of this article.

Acknowledgment

The authors gratefully acknowledge ProteinsInsights, Nangal Raya, New Delhi, India, for providing the computational resources essential for the successful completion of this research.

Disclosure statement

No potential conflict of interest was reported by the author(s).

References

- AlAjmi, M. F., Rehman, M. T., Hussain, A., & Rather, G. M. (2018). Pharmacoinformatics approach for the identification of Polo-like kinase-1 inhibitors from natural sources as anti-cancer agents. *International Journal of Biological Macromolecules*, *116*, 173–181. <https://doi.org/10.1016/j.ijbiomac.2018.05.023>
- Arai, Y., Nakazato, K., Kinemuchi, H., Tadano, T., Satoh, N., Oyama, K., & Kisara, K. (1991). Inhibition of rat brain monoamine oxidase activity by cerebral anti-ischemic agent, ifenprodil. *Neuropharmacology*, *30*(7), 809–812. [https://doi.org/10.1016/0028-3908\(91\)90190-m](https://doi.org/10.1016/0028-3908(91)90190-m)
- Barnham, K. J., Masters, C. L., & Bush, A. I. (2004). Neurodegenerative diseases and oxidative stress. *Nature Reviews. Drug Discovery*, *3*(3), 205–214. <https://doi.org/10.1038/nrd1330>
- Benson, N. C., & Daggett, V. (2012). A comparison of multiscale methods for the analysis of molecular dynamics simulations. *The Journal of Physical Chemistry-B*, *116*(29), 8722–8731. <https://doi.org/10.1021/jp302103t>
- Bhandari, S., Agrwal, A., Kasana, V., Tandon, S., Boulaamane, Y., & Maurady, A. (2022). β -amino carbonyl derivatives: Synthesis, molecular docking, ADMET, molecular dynamic and herbicidal studies. *ChemistrySelect*, *7*(48), e202201572. <https://doi.org/10.1002/slct.202201572>
- Bharadwaj, K. K., Sarkar, T., Ghosh, A., Baishya, D., Rabha, B., Panda, M. K., Nelson, B. R., John, A. B., Sheikh, H. I., Dash, B. P., Edinur, H. A., & Pati, S. (2021). Macrolactin A as a novel inhibitory agent for SARS-CoV-2 M pro: Bioinformatics approach. *Applied Biochemistry and Biotechnology*, *193*(10), 3371–3394. <https://doi.org/10.1007/s12010-021-03608-7>
- Binda, C., Mattevi, A., & Edmondson, D. E. (2011). Structural properties of human monoamine oxidases A and B. *International Review of Neurobiology*, *100*, 1–11.
- Binda, C., Wang, J., Pisani, L., Caccia, C., Carotti, A., Salvati, P., Edmondson, D. E., & Mattevi, A. (2007). Structures of human monoamine oxidase B complexes with selective noncovalent inhibitors: Safinamide and coumarin analogs. *Journal of Medicinal Chemistry*, *50*(23), 5848–5852. <https://doi.org/10.1021/jm070677y>
- Boulaamane, Y., Ahmad, I., Patel, H., Das, N., Britel, M. R., & Maurady, A. (2023). Structural exploration of selected C6 and C7-substituted coumarin isomers as selective MAO-B inhibitors. *Journal of Biomolecular Structure & Dynamics*, *41*(6), 2326–2340. <https://doi.org/10.1080/07391102.2022.2033643>
- Boulaamane, Y., Ibrahim, M. A., Britel, M. R., & Maurady, A. (2022). *In silico* studies of natural product-like caffeine derivatives as potential MAO-B inhibitors/AA2AR antagonists for the treatment of Parkinson's disease. *Journal of Integrative Bioinformatics*, *19*(4), 20210027. <https://doi.org/10.1515/jib-2021-0027>
- Boulaamane, Y., Kandpal, P., Chandra, A., Britel, M. R., & Maurady, A. (2023). Chemical library design, QSAR modeling and molecular dynamics simulations of naturally occurring coumarins as dual inhibitors of MAO-B and AChE. *Journal of Biomolecular Structure & Dynamics*, 1–18. <https://doi.org/10.1080/07391102.2023.2209650>
- Bowers, K. J., Chow, E., Xu, H., Dror, R. O., Eastwood, M. P., Gregersen, B. A., ... Shaw, D. E. (2006). Scalable algorithms for molecular dynamics simulations on commodity clusters. In Proceedings of the 2006 ACM/IEEE Conference on Supercomputing, November. (pp. 84–es). <https://doi.org/10.1145/1188455.1188544>
- Burggraaff, L., van Vlijmen, H. W. T., IJzerman, A. P., & van Westen, G. J. P. (2020). Quantitative prediction of selectivity between the A1 and A2A adenosine receptors. *Journal of Cheminformatics*, *12*(1), 33. <https://doi.org/10.1186/s13321-020-00438-3>
- Carradori, S., D'Ascenzio, M., Chimenti, P., Secci, D., & Bolasco, A. (2014). Selective MAO-B inhibitors: A lesson from natural products. *Molecular Diversity*, *18*(1), 219–243. <https://doi.org/10.1007/s11030-013-9490-6>
- Carradori, S., & Silvestri, R. (2015). New frontiers in selective human MAO-B inhibitors: Miniperspective. *Journal of Medicinal Chemistry*, *58*(17), 6717–6732. <https://doi.org/10.1021/jm501690r>
- Craft, R. C., & Leake, C. (2002). The Pareto principle in organizational decision making. *Management Decision*, *40*(8), 729–733. <https://doi.org/10.1108/00251740210437699>
- Dauer, W., & Przedborski, S. (2003). Parkinson's disease: Mechanisms and models. *Neuron*, *39*(6), 889–909. [https://doi.org/10.1016/s0896-6273\(03\)00568-3](https://doi.org/10.1016/s0896-6273(03)00568-3)
- David, C. C., & Jacobs, D. J. (2014). Principal component analysis: A method for determining the essential dynamics of proteins. *Method in Molecular Biology*, *1084*, 193–226.
- de Lera Ruiz, M., Lim, Y. H., & Zheng, J. (2014). Adenosine A2A receptor as a drug discovery target. *Journal of Medicinal Chemistry*, *57*(9), 3623–3650. <https://doi.org/10.1021/jm4011669>
- Ding, Y., Chen, M., Guo, C., Zhang, P., & Wang, J. (2021). Molecular fingerprint-based machine learning assisted QSAR model development for prediction of ionic liquid properties. *Journal of Molecular Liquids*, *326*, 115212. <https://doi.org/10.1016/j.molliq.2020.115212>

- Dixon, S. L., Smondyrev, A. M., & Rao, S. N. (2006). PHASE: A novel approach to pharmacophore modeling and 3D database searching. *Chemical Biology & Drug Design*, 67(5), 370–372. <https://doi.org/10.1111/j.1747-0285.2006.00384.x>
- Erdogan Orhan, I. (2016). Potential of natural products of herbal origin as monoamine oxidase inhibitors. *Current Pharmaceutical Design*, 22(3), 268–276. <https://doi.org/10.2174/1381612822666151112150612>
- Finberg, J. P., & Rabey, J. M. (2016). Inhibitors of MAO-A and MAO-B in psychiatry and neurology. *Frontiers in Pharmacology*, 7, 340. <https://doi.org/10.3389/fphar.2016.00340>
- Fjellidal, M. F., Freyd, T., Evenseth, L. M., Sylte, I., Ring, A., & Paulsen, R. E. (2019). Exploring the overlapping binding sites of ifenprodil and EVT-101 in GluN2B-containing NMDA receptors using novel chicken embryo forebrain cultures and molecular modeling. *Pharmacology Research & Perspectives*, 7(3), e00480. <https://doi.org/10.1002/prp2.480>
- Friesner, R. A., Murphy, R. B., Repasky, M. P., Frye, L. L., Greenwood, J. R., Halgren, T. A., Sanschagrin, P. C., & Mainz, D. T. (2006). Extra precision glide: Docking and scoring incorporating a model of hydrophobic enclosure for protein–ligand complexes. *Journal of Medicinal Chemistry*, 49(21), 6177–6196. <https://doi.org/10.1021/jm051256o>
- Gaulton, A., Bellis, L. J., Bento, A. P., Chambers, J., Davies, M., Hersey, A., Light, Y., McGlinchey, S., Michalovich, D., Al-Lazikani, B., & Overington, J. P. (2012). ChEMBL: A large-scale bioactivity database for drug discovery. *Nucleic Acids Research*, 40(Database issue), D1100–D1107. <https://doi.org/10.1093/nar/gkr777>
- Gonda, X. (2012). Basic pharmacology of NMDA receptors. *Current Pharmaceutical Design*, 18(12), 1558–1567. <https://doi.org/10.2174/138161212799958521>
- Gulli, A., & Pal, S. (2017). *Deep learning with Keras*. Packt Publishing Ltd.
- Hanley, J. A., & McNeil, B. J. (1982). The meaning and use of the area under a receiver operating characteristic (ROC) curve. *Radiology*, 143(1), 29–36. <https://doi.org/10.1148/radiology.143.1.7063747>
- Hardingham, G. E. (2009). Coupling of the NMDA receptor to neuroprotective and neurodestructive events. *Biochemical Society Transactions*, 37(Pt 6), 1147–1160. <https://doi.org/10.1042/BST0371147>
- He, X., Walker, B., Man, V. H., Ren, P., & Wang, J. (2022). Recent progress in general force fields of small molecules. *Current Opinion in Structural Biology*, 72, 187–193. <https://doi.org/10.1016/j.sbi.2021.11.011>
- Herrera-Acevedo, C., Perdomo-Madriral, C., Herrera-Acevedo, K., Coy-Barrera, E., Scotti, L., & Scotti, M. T. (2021). Machine learning models to select potential inhibitors of acetylcholinesterase activity from Sistemax: A natural products database. *Molecular Diversity*, 25(3), 1553–1568. <https://doi.org/10.1007/s11030-021-10245-z>
- Ibrahim, M. M., & Gabr, M. T. (2019). Multitarget therapeutic strategies for Alzheimer's disease. *Neural Regeneration Research*, 14(3), 437–440. <https://doi.org/10.4103/1673-5374.245463>
- Ikedda, K., Kurokawa, M., Aoyama, S., & Kuwana, Y. (2002). Neuroprotection by adenosine A2A receptor blockade in experimental models of Parkinson's disease. *Journal of Neurochemistry*, 80(2), 262–270. <https://doi.org/10.1046/j.0022-3042.2001.00694.x>
- Ioakimidis, L., Thoukydidis, L., Mirza, A., Naeem, S., & Reynisson, J. (2008). Benchmarking the reliability of QikProp. Correlation between experimental and predicted values. *QSAR & Combinatorial Science*, 27(4), 445–456. <https://doi.org/10.1002/qsar.200730051>
- Iovino, L., Tremblay, M. E., & Civiero, L. (2020). Glutamate-induced excitotoxicity in Parkinson's disease: The role of glial cells. *Journal of Pharmacological Sciences*, 144(3), 151–164. <https://doi.org/10.1016/j.jphs.2020.07.011>
- Jaakola, V. P., Lane, J. R., Lin, J. Y., Katritch, V., IJzerman, A. P., & Stevens, R. C. (2010). Ligand binding and subtype selectivity of the human A2A adenosine receptor: Identification and characterization of essential amino acid residues. *The Journal of Biological Chemistry*, 285(17), 13032–13044. <https://doi.org/10.1074/jbc.M109.096974>
- Jacobson, M. P., Friesner, R. A., Xiang, Z., & Honig, B. (2002). On the role of the crystal environment in determining protein side-chain conformations. *Journal of Molecular Biology*, 320(3), 597–608. [https://doi.org/10.1016/s0022-2836\(02\)00470-9](https://doi.org/10.1016/s0022-2836(02)00470-9)
- Jacobson, M. P., Pincus, D. L., Rapp, C. S., Day, T. J., Honig, B., Shaw, D. E., & Friesner, R. A. (2004). A hierarchical approach to all-atom protein loop prediction. *Proteins*, 55(2), 351–367. <https://doi.org/10.1002/prot.10613>
- Jaiteh, M., Zeifman, A., Saarinen, M., Svenningsson, P., Bréa, J., Loza, M. I., & Carlsson, J. (2018). Docking screens for dual inhibitors of disparate drug targets for Parkinson's disease. *Journal of Medicinal Chemistry*, 61(12), 5269–5278. <https://doi.org/10.1021/acs.jmedchem.8b00204>
- Jenner, P. (2003). Oxidative stress in Parkinson's disease. *Annals of Neurology*, 53(Suppl S3), S26–S38. <https://doi.org/10.1002/ana.10483>
- Ke, Q., Gong, X., Liao, S., Duan, C., & Li, L. (2022). Effects of thermostats/barostats on physical properties of liquids by molecular dynamics simulations. *Journal of Molecular Liquids*, 365, 120116. <https://doi.org/10.1016/j.molliq.2022.120116>
- Kim, S., Chen, J., Cheng, T., Gindulyte, A., He, J., He, S., Li, Q., Shoemaker, B. A., Thiessen, P. A., Yu, B., Zaslavsky, L., Zhang, J., & Bolton, E. E. (2021). PubChem in 2021: New data content and improved web interfaces. *Nucleic Acids Research*, 49(D1), D1388–D1395. <https://doi.org/10.1093/nar/gkaa971>
- Kingston, D. G. (2011). Modern natural products drug discovery and its relevance to biodiversity conservation. *Journal of Natural Products*, 74(3), 496–511. <https://doi.org/10.1021/np100550t>
- Kumar, G., & Patnaik, R. (2016). Exploring neuroprotective potential of *Withania somnifera* phytochemicals by inhibition of GluN2B-containing NMDA receptors: An *in silico* study. *Medical Hypotheses*, 92, 35–43. <https://doi.org/10.1016/j.mehy.2016.04.034>
- Kurczab, R., Ali, W., Łażewska, D., Kotańska, M., Jastrzębska-Więsek, M., Satała, G., Więcek, M., Lubelska, A., Latacz, G., Partyka, A., Starek, M., Dąbrowska, M., Wesołowska, A., Jacob, C., Kieć-Kononowicz, K., & Handzlik, J. (2018). Computer-aided studies for novel arylhydantoin 1, 3, 5-triazine derivatives as 5-HT₆ serotonin receptor ligands with anti-depressive-like, anxiolytic and antiobesity action *in vivo*. *Molecules*, 23(10), 2529. <https://doi.org/10.3390/molecules23102529>
- Landrum, G. (2013). RDKit: A software suite for cheminformatics, computational chemistry, and predictive modeling. *Greg Landrum*, 8, 31.
- Lang, A. E. (2010). Clinical trials of disease-modifying therapies for neurodegenerative diseases: The challenges and the future. *Nature Medicine*, 16(11), 1223–1226. <https://doi.org/10.1038/nm.2220>
- Lin, J., Sahakian, D. C., De Moraes, S. M., Xu, J. J., Polzer, R. J., & Winter, S. M. (2003). The role of absorption, distribution, metabolism, excretion and toxicity in drug discovery. *Current Topics in Medicinal Chemistry*, 3(10), 1125–1154. <https://doi.org/10.2174/1568026033452096>
- Lipinski, C. A. (2004). Lead-and drug-like compounds: The rule-of-five revolution. *Drug Discovery Today. Technologies*, 1(4), 337–341. <https://doi.org/10.1016/j.ddtec.2004.11.007>
- Lotharius, J., & Brundin, P. (2002). Pathogenesis of Parkinson's disease: Dopamine, vesicles and α -synuclein. *Nature Reviews. Neuroscience*, 3(12), 932–942. <https://doi.org/10.1038/nrn983>
- Maestro, S. (2020). Maestro. Schrödinger, LLC, New York, NY, 2020.
- Milczek, E. M., Binda, C., Rovida, S., Mattevi, A., & Edmondson, D. E. (2011). The 'gating' residues Ile199 and Tyr326 in human monoamine oxidase B function in substrate and inhibitor recognition. *The FEBS Journal*, 278(24), 4860–4869. <https://doi.org/10.1111/j.1742-4658.2011.08386.x>
- Mironova, Y. S., Zhukova, I. A., Zhukova, N. G., Alifirova, V. M., Izhboldina, O. P., & Latypova, A. V. (2018). Parkinson's disease and glutamate excitotoxicity. *Zhurnal nevrologii i psikiatrii imeni S.S. Korsakova*, 118(6. Vyp. 2), 50–54. <https://doi.org/10.17116/jnevro201811806250>
- Ng, H. W., Laughton, C. A., & Doughty, S. W. (2013). Molecular dynamics simulations of the adenosine A2a receptor: Structural stability, sampling, and convergence. *Journal of Chemical Information and Modeling*, 53(5), 1168–1178. <https://doi.org/10.1021/ci300610w>
- Olsson, M. H., Søndergaard, C. R., Rostkowski, M., & Jensen, J. H. (2011). PROPKA3: Consistent treatment of internal and surface residues in empirical pKa predictions. *Journal of Chemical Theory and Computation*, 7(2), 525–537. <https://doi.org/10.1021/ct100578z>
- Pedregosa, F., Varoquaux, G., Gramfort, A., Michel, V., Thirion, B., Grisel, O., & Duchesnay, E. (2011). Scikit-learn: Machine learning in Python. *The Journal of Machine Learning Research*, 12, 2825–2830.
- Piau, A., Nourhashemi, F., Hein, C., Caillaud, C., & Vellas, B. (2011). Progress in the development of new drugs in Alzheimer's disease. *The*

- Journal of Nutrition, Health & Aging*, 15(1), 45–57. <https://doi.org/10.1007/s12603-011-0012-x>
- Pollastri, M. P. (2010). Overview on the rule of five. *Current Protocols in Pharmacology*, 9(1), Unit 9.12. <https://doi.org/10.1002/0471141755.ph0912s49>
- Rascol, O., Payoux, P., Ory, F., Ferreira, J. J., Brefel-Courbon, C., & Montastruc, J. L. (2003). Limitations of current Parkinson's disease therapy. *Annals of Neurology*, 53(Suppl. 3), S3–S15. <https://doi.org/10.1002/ana.10513>
- Roos, K., Wu, C., Damm, W., Reboul, M., Stevenson, J. M., Lu, C., Dahlgren, M. K., Mondal, S., Chen, W., Wang, L., Abel, R., Friesner, R. A., & Harder, E. D. (2019). OPLS3e: Extending force field coverage for drug-like small molecules. *Journal of Chemical Theory and Computation*, 15(3), 1863–1874. <https://doi.org/10.1021/acs.jctc.8b01026>
- Sander, T., Freyss, J., von Korff, M., & Rufener, C. (2015). DataWarrior: An open-source program for chemistry aware data visualization and analysis. *Journal of Chemical Information and Modeling*, 55(2), 460–473. <https://doi.org/10.1021/ci500588j>
- Segala, E., Guo, D., Cheng, R. K. Y., Bortolato, A., Deflorian, F., Doré, A. S., Errey, J. C., Heitman, L. H., Ilzerman, A. P., Marshall, F. H., & Cooke, R. M. (2016). Controlling the dissociation of ligands from the adenosine A2A receptor through modulation of salt bridge strength. *Journal of Medicinal Chemistry*, 59(13), 6470–6479. <https://doi.org/10.1021/acs.jmedchem.6b00653>
- Shen, B. (2015). A new golden age of natural products drug discovery. *Cell*, 163(6), 1297–1300. <https://doi.org/10.1016/j.cell.2015.11.031>
- Singh, P., Manure, A., Singh, P., & Manure, A. (2020). Introduction to tensorflow 2.0. Learn Tensor Flow 2.0: Implement Machine Learning and Deep Learning Models with Python, 1–24.
- Sorokina, M., Merseburger, P., Rajan, K., Yirik, M. A., & Steinbeck, C. (2021). COCONUT online: Collection of open natural products database. *Journal of Cheminformatics*, 13(1), 2. <https://doi.org/10.1186/s13321-020-00478-9>
- Stocchi, F., Antonini, A., Berg, D., Bergmans, B., Jost, W., Katzenschlager, R., Kulisevsky, J., Odin, P., Valdeoriola, F., & Ray Chaudhuri, K. (2022). Safinamide in the treatment pathway of Parkinson's disease: A European Delphi consensus. *NPJ Parkinson's Disease*, 8(1), 17. <https://doi.org/10.1038/s41531-022-00277-z>
- Stoof, J. C., Booij, J., & Drukarch, B. (1992). Amantadine as N-methyl-D-aspartic acid receptor antagonist: New possibilities for therapeutic applications? *Clinical Neurology and Neurosurgery*, 94, 54–56. [https://doi.org/10.1016/0303-8467\(92\)90006-o](https://doi.org/10.1016/0303-8467(92)90006-o)
- Stroebel, D., Buhl, D. L., Knafels, J. D., Chanda, P. K., Green, M., Sciabola, S., Mony, L., Paoletti, P., & Pandit, J. (2016). A novel binding mode reveals two distinct classes of NMDA receptor GluN2B-selective antagonists. *Molecular Pharmacology*, 89(5), 541–551. <https://doi.org/10.1124/mol.115.103036>
- Tabakman, R., Lecht, S., & Lazarovici, P. (2004). Neuroprotection by monoamine oxidase B inhibitors: A therapeutic strategy for Parkinson's disease? *BioEssays*, 26(1), 80–90. <https://doi.org/10.1002/bies.10378>
- Tarasova, O. A., Urusova, A. F., Filimonov, D. A., Nicklaus, M. C., Zakharov, A. V., & Poroikov, V. V. (2015). QSAR modeling using large-scale databases: Case study for HIV-1 reverse transcriptase inhibitors. *Journal of Chemical Information and Modeling*, 55(7), 1388–1399. <https://doi.org/10.1021/acs.jcim.5b00019>
- The UniProt Consortium. (2021). UniProt: The universal protein knowledgebase in 2021. *Nucleic Acids Research*, 49(D1), D480–D489. <https://doi.org/10.1093/nar/gkaa1100>
- Touati, I., Abdalla, M., Ali, N. H., AlRuwaiti, R., Alruwaiti, M., Britel, M. R., & Maurady, A. (2023). Constituents of Stachys plants as potential dual inhibitors of AChE and NMDAR for the treatment of Alzheimer's disease: A molecular docking and dynamic simulation study. *Journal of Biomolecular Structure & Dynamics*, 1–17. <https://doi.org/10.1080/07391102.2023.2217925>
- Van der Maaten, L., & Hinton, G. (2008). Visualizing data using t-SNE. *Journal of Machine Learning Research*, 9(11), 2579–2605.
- Van der Schyf, C. J. (2011). The use of multi-target drugs in the treatment of neurodegenerative diseases. *Expert Review of Clinical Pharmacology*, 4(3), 293–298. <https://doi.org/10.1586/ecp.11.13>
- Wang, C. C., Billett, E., Borchert, A., Kuhn, H., & Ufer, C. (2013). Monoamine oxidases in development. *Cellular and Molecular Life Sciences*, 70(4), 599–630. <https://doi.org/10.1007/s00018-012-1065-7>
- Wang, M., Hou, S., Wei, Y., Li, D., & Lin, J. (2021). Discovery of novel dual adenosine A1/A2A receptor antagonists using deep learning, pharmacophore modeling and molecular docking. *PLOS Computational Biology*, 17(3), e1008821. <https://doi.org/10.1371/journal.pcbi.1008821>
- Welihinda, A. A., Kaur, M., Greene, K., Zhai, Y., & Amento, E. P. (2016). The adenosine metabolite inosine is a functional agonist of the adenosine A2A receptor with a unique signaling bias. *Cellular Signalling*, 28(6), 552–560. <https://doi.org/10.1016/j.cellsig.2016.02.010>
- Williams, K. (2001). Ifenprodil, a novel NMDA receptor antagonist: Site and mechanism of action. *Current Drug Targets*, 2(3), 285–298. <https://doi.org/10.2174/1389450013348489>
- Wu, Z., Zhu, M., Kang, Y., Leung, E. L.-H., Lei, T., Shen, C., Jiang, D., Wang, Z., Cao, D., & Hou, T. (2021). Do we need different machine learning algorithms for QSAR modeling? A comprehensive assessment of 16 machine learning algorithms on 14 QSAR data sets. *Briefings in Bioinformatics*, 22(4), bbaa321. <https://doi.org/10.1093/bib/bbaa321>
- Yamada, M., & Yasuhara, H. (2004). Clinical pharmacology of MAO inhibitors: safety and future. *Neurotoxicology*, 25(1-2), 215–221.
- Yang, S., Li, S., & Chang, J. (2022). Discovery of Cobimetinib as a novel A-FABP inhibitor using machine learning and molecular docking-based virtual screening. *RSC Advances*, 12(21), 13500–13510. <https://doi.org/10.1039/d2ra01057g>
- Youdim, M. B., Edmondson, D., & Tipton, K. F. (2006). The therapeutic potential of monoamine oxidase inhibitors. *Nature Reviews. Neuroscience*, 7(4), 295–309. <https://doi.org/10.1038/nrn1883>
- Zhang, Z., Zhang, S., Fu, P., Zhang, Z., Lin, K., Ko, J. K. S., & Yung, K. K. L. (2019). Roles of glutamate receptors in Parkinson's disease. *International Journal of Molecular Sciences*, 20(18), 4391. <https://doi.org/10.3390/ijms20184391>